Stockholm University

Stimuli-Responsive Materials Derived from Cellulose Nanofibrils

Synthesis, characterization, and performance evaluation

Frédéric Héraly

Doctoral Thesis in Materials Chemistry at Stockholm University, Sweden 2024

Stimuli-Responsive Materials Derived from Cellulose Nanofibrils

Synthesis, characterization, and performance evaluation

Frédéric Héraly

Academic dissertation for the Degree of Doctor of Philosophy in Materials Chemistry at Stockholm University to be publicly defended on Friday 16 February 2024 at 13.00 in Magnélisalen, Kemiska övningslaboratoriet, Svante Arrhenius väg 16 B.

Abstract

This thesis presents a comprehensive study on stimuli-responsive materials derived from cellulose nanofibrils (CNFs), focusing on their synthesis, characterization, and performance evaluation in various applications. Renowned for their biodegradability, renewability, and robust mechanical properties, CNFs are explored in three primary contexts: moisture-responsive actuators, voltage-responsive actuators, and CO_2-responsive sensors.

The unique properties of CNFs, such as high tensile strength and surface area, are leveraged to achieve effective motion in response to moisture exposure. Specifically, CNFs are utilized to create bilayer, torsional, and tensile actuators. These actuators exhibit controllable and dynamic responses, making them suitable for applications in soft robotics and wearable technology.

In the realm of voltage-responsive actuators, this study investigates the impact of various electrolytes and counteranions on positively charged CNFs. It uncovers the critical role of electrolyte choice, ion migration and the plasticization effect within the CNFs matrix, resulting in volumetric expansion, which is pivotal to the actuation mechanism. These insights pave the way for CNFs applications requiring precise control of motion and flexibility in shape, such as in soft robotics.

The third area of application involves the development of a capacitive CO_2 sensor using CNFs-based foams functionalized with primary amines to enhance CO_2 capture through chemisorption. This functionalization turns the CNFs-based foam into an efficient dielectric layer (DE) for sensor applications. The addition of 1,8-diazabicyclo[5.4.0]undec-7-ene (DBU) to the DE further expands the scope of sensor's capacitance change in response to CO_2 exposure, underscoring its potential in environmental monitoring and CO_2 detection.

Overall, this thesis emphasizes the versatility and adaptability of CNFs as a sustainable biomaterial for developing stimuli-responsive devices. The insights gained from studying CNFs in these varied applications contribute significantly to materials science and open new avenues for research in sustainable, bio-based materials.

Keywords: *bio-based materials, cellulose nanofibrils, CO_2 sorption, soft actuators, stimuli-responsive materials.*

Stockholm 2024
http://urn.kb.se/resolve?urn=urn:nbn:se:su:diva-224538

ISBN 978-91-8014-627-2
ISBN 978-91-8014-628-9

Department of Materials and Environmental Chemistry (MMK)

Stockholm University, 106 91 Stockholm

Stockholm University

STIMULI-RESPONSIVE MATERIALS DERIVED FROM CELLULOSE NANOFIBRILS

Frédéric Héraly

Stockholm University

Stimuli-Responsive Materials Derived from Cellulose Nanofibrils

Synthesis, characterization, and performance evaluation

Frédéric Héraly

ISBN print 978-91-8014-627-2
ISBN PDF 978-91-8014-628-9

The cover picture is a personal creation entitled A **Scandinavian Symphony**.

Printed in Sweden by Universitetsservice US-AB, Stockholm 2024

To my family,
for the infinite love &
support.

Abstract

This thesis presents a comprehensive study on stimuli-responsive materials derived from cellulose nanofibrils (CNFs), focusing on their synthesis, characterization, and performance evaluation in various applications. Renowned for their biodegradability, renewability, and robust mechanical properties, CNFs are explored in three primary contexts: moisture-responsive actuators, voltage-responsive actuators, and CO_2-responsive sensors.

The unique properties of CNFs, such as high tensile strength and surface area, are leveraged to achieve effective motion in response to moisture exposure. Specifically, CNFs are utilized to create bilayer, torsional, and tensile actuators. These actuators exhibit controllable and dynamic responses, making them suitable for applications in soft robotics and wearable technology.

In the realm of voltage-responsive actuators, this study investigates the impact of various electrolytes and counteranions on positively charged CNFs. It uncovers the critical role of electrolyte choice, ion migration and the plasticization effect within the CNFs matrix, resulting in volumetric expansion, which is pivotal to the actuation mechanism. These insights pave the way for CNFs applications requiring precise control of motion and flexibility in shape, such as in soft robotics.

The third area of application involves the development of a capacitive CO_2 sensor using CNFs-based foams functionalized with primary amines to enhance CO_2 capture through chemisorption. This functionalization turns the CNFs-based foam into an efficient dielectric layer (DE) for sensor applications. The addition of 1,8-diazabicyclo[5.4.0]undec-7-ene (DBU) to the DE further expands the scope of sensor's capacitance change in response to CO_2 exposure, underscoring its potential in environmental monitoring and CO_2 detection.

Overall, this thesis emphasizes the versatility and adaptability of CNFs as a sustainable biomaterial for developing stimuli-responsive devices. The insights gained from studying CNFs in these varied applications contribute significantly to materials science and open new avenues for research in sustainable, bio-based materials.

Sammanfattning

Denna avhandling presenterar en omfattande studie om stimuli-reaktiva material tillverkade av cellulosa nanofibriller (CNFer), med särskilt fokus på dess syntes, karaktärisering, och prestandautvärdering i olika applikationer. CNFer är kända för att vara biologiskt nedbrytbara, förnybara och ha robusta mekaniska egenskaper. I studien utforskas tre huvudområden: fuktaktiverade aktuatorer, spänningsaktiverade aktuatorer och CO_2-reaktiva sensorer.

De unika egenskaperna hos CNFer, såsom hög draghållfasthet och ytspänning, utnyttjas för att skapa effektiva rörelser som svar på fuktexponering. Specifikt används CNFer för att utveckla dubbellager-, vridnings- och dragaktuatorer. Dessa ställdon demonstrerar snabba och dynamiska reaktioner, vilket gör dem idealiska för användning i kroppsnära teknologi.

Inom området för spänningsreaktiva aktuatorer utforskar denna studie effekten av olika elektrolyter och motjoner på positivt laddade CNFer. Forskning visar att valet av elektrolyter har stor påverkan på, jonmigration och plastiseringseffekter hos CNF-matriserna; något som i sin tur bidrar till volymexpansion vilket är en central del i aktueringsmekanismen. Dessa insikter öppnar nya tillämpningsområden för CNFer som kräver noggrann kontroll och flexibilitet, exempelvis inom mjuk robotik.

Det tredje tillämpningsområdet omfattar utvecklingen av CO_2-sensorer gjorda av CNF-baserat skum som funktionaliserats med primära aminer. Detta förbättrar CO_2-upptaget genom kemisk absorptionoch gör CNF-baserat skum till ett effektivt dielektriskt lager för sensortillämpningar. Tillsats av DBU till det dielektriska lagert förbättrar sensorns förmåga att ändra kapacitans som svar på CO_2-exponering, vilket understryker dess potential inom miljöövervakning och CO_2-detektering.

Sammanfattningsvis visar denna avhandling på mångsidigheten och anpassningsförmågan hos CNFer som ett hållbart material för utveckling av stimulireaktiva enheter. De insikter som vunnits från studier av CNFer i dessa varierande tillämpningar bidrar avsevärt till materialvetenskapen och öppnar nya vägar för forskning inom hållbara biomaterial.

Populärvetenskaplig sammanfattning

Denna avhandling fokuserar på utveckling och analys av stimuli-reaktiva material baserade på cellulosa nanofibriller (CNFer), och täcker tre huvudområden: fuktaktiverade aktuatorer, spänningsaktiverade aktuatorer och CO_2-reaktiva sensorer. CNFer är kända för sina miljövänliga och starka mekaniska egenskaper är centrala i denna forskning. Fuktreaktiva aktuatorer eller ställdon utvecklade från CNFer uppvisar snabb respons på fuktexponering, vilket gör dem användbara inom exempelvis kroppsnära teknologi. Inom spänningsreaktiva aktuatorer, utforskas interaktionen mellan positivt laddade CNFer och olika elektrolyter, vilket leder till nya insikter om kopplingen mellan volymexpansion och aktueringsmekanismer vilket är relevant för applikationer inom mjuk robotik. Slutligen presenteras en kapacitiv CO_2-sensor som använder CNF-baserat skum funktionaliserat med primära aminer för effektiv CO_2-uppfångning vilket öppnar nya möjligheter för miljöövervakning. Denna avhandling bidrar avsevärt till förståelsen av CNFers potential i skapandet av hållbara och stimuli-reaktiva enheter, och markerar ett viktigt steg framåt för forskningen inom hållbara, bio-material.

List of publications

This thesis is written based on the following publications:

Paper I.

Nanodancing with moisture: Humidity-sensitive bilayer actuator derived from cellulose nanofibrils and reduced graphene oxide

Frédéric Héraly, Miao Zhang, Agnes Åhl, Wei Cao, Lennart Bergström and Jiayin Yuan. Advanced Intelligent Systems (2021) **4**, 2100084.

My contributions to this project included conceptualization, investigation, methodology, validation, and the original draft preparation. I was instrumental in the project planning, conducted the majority of the experiments, and took a leading role in manuscript development.

Paper II.

Cationic cellulose nanofibrils-based electro-actuators: the effects of counteranion and electrolyte

Frédéric Héraly, Bo Pang and Jiayin Yuan. Sensors and Actuators Reports (2023) **5**, 100142.

My contributions included conceptualizing the research idea, conducting the majority of experiments, and writing most of the manuscript, encompassing investigation, methodology, and validation aspects.

Paper III.

Capacitive CO_2 sensor made of aminated cellulose nanofibrils: Development and optimization

Frédéric Héraly, Anirban Sikdar, Jian Chang and Jiayin Yuan. Submitted manuscript (2024).

My role encompassed the conceptualization of the research idea, and I conducted the majority of the experiments, which included investigation, methodology, and validation.

Paper IV.

Humidity-responsive fiber actuators assembled from cellulose nanofibrils

Frédéric Héraly, Anirban Sikdar, Jian Chang, Bo Pang and Jiayin Yuan. Submitted manuscript (2024).

My contributions included conceptualizing the project, performing the majority of experiments which encompassed investigation, methodology, and validation.

Publications not included in this thesis :

I. A transport channel-regulated MXene membrane via organic phosphonic acids for efficient water permeation
Ming Yi, Frédéric Héraly, Jian Chang, Atefeh Kheirabad, Jiayin Yuan, Yonglei Wang and Miao Zhang. Chemical Communications (2021) 51, 6245-6248.

My contribution involved participating in the experimental work and writing of part of the original manuscript.

II. Multitasking tartaric-acid-enabled, highly conductive, and stable MXene/conducting polymer composite for ultrafast supercapacitor

Miao Zhang, Frédéric Héraly, Ming Yi and Jiayin Yuan. Cell Reports Physical Science (2022) 6, 100449

My contribution included participating in the experimental part, and the preparation of part of the original manuscript.

III. Vacancy-rich MXene-immobilized Ni single atom as high-performance electrocatalyst for hydrazine oxidation reaction

Shiqi Zhou, Yunxuan Zhao, Run Shi, Yucheng Wang, Anumol Ashok, Frédéric Héraly, Tierui Zhang and Jiayin Yuan. Advanced Materials (2022), 2204388.

My contribution involved participating in the experimental work and revision of the original manuscript.

IV. Polypeptide-based vapor-responsive porous poly (ionic liquid) actuators: From reversible to unexpectedly irreversible actuation

Shuhe Wei, Yan Xiao, Hanwen Jiang, Frédéric Héraly, Liangshun Zhang, Wanyi Huang, Jiayin Yuan, Meidong Lang. Materials Today Communications (2023), 35, 105878.

My contribution included participating in the conceptualization, scientific discussion, data analysis, and edition and revision of the original manuscript.

V. Hierarchically porous 3D freestanding holey-MXene framework *via* mild oxidation of self-assembled MXene hydrogel for ultrafast pseudocapacitive energy storage

Anirban Sikdar, Frédéric Héraly, Hao Zhang, Stephen Hall, Kanglei Pang, Miao Zhang, Jiayin Yuan. Accepted manuscript (2024).

My contribution involved participating in the experimental work and edition of the original manuscript.

Original work declaration for Figures and Photos

Unless explicitly indicated otherwise, all figures and photographs included in this thesis are the original work of the author. These visuals have been created, captured, and developed as part of the research conducted during the course of this PhD study.

Abbreviations

AFM	Atomic force microscopy
APDEMS	3-Aminopropyldiethoxymethylsilane
BET	Brunauer-Emmet-Teller
BF_4^-	Tetrafluoroborate anion
Cl^-	Chloride anion
CNFs	Cellulose nanofibrils
DBU	1,8-Diazabicyclo(5.4.0)undec-7-ene
EDS	Energy-dispersive X-ray spectroscopy
FD	Freeze-dried
FTIR	Fourier-transform infrared spectroscopy
GO	Graphene oxide
IL	Ionic liquid
PF_6^-	Hexafluorophosphate anion
PVDF	Polyvinylidene fluoride
PXRD	Powder X-ray diffraction
rGO	Reduced graphene oxide
RH	Relative humidity
SEM	Scanning electron microscopy
TCNFs-Na^+	TEMPO-oxidized cellulose nanofibrils with Na^+ cation
TEMPO	2,2,6,6-Tetramethylpiperidin-1-oxyl radical
$TFSI^-$	Bis(trifluoromethanesulfonyl)imide
TGA	Thermogravimetric analysis
Wt%	Weight percent
XRD	X-ray diffraction

Contents

1. Introduction

In addressing the diverse challenges our society faces, from environmental issues to advancement of technologies, there is a growing recognition of the need for materials that are innovative and sustainable. Among various options, stimuli-responsive materials,[1,2] especially those based on cellulose nanofibrils, are being considered as a potential solution.[3] Their distinct physicochemical properties and adaptability to environments offer a way to meet the increasing demands for materials that balance technological progress with sustainability.[4]

1.1 Motivation

Cellulose, the most abundant biopolymer on Earth,[5] has gained significant attention in materials science owing to its innovative potential.[6] Commonly found in plant cell walls and primarily extracted from trees, cellulose is also abundant in other plant-based materials such as cotton fibers, hemp, and bamboo.[7] These diverse sources underscore its versatility and wide availability, making it a key component in sustainable materials development.[8] Distinctive features of cellulose include biodegradability, renewability, and robust mechanical properties. On a molecular level, cellulose consists of linearly arranged repeating glucose units, linked by β (1→4) glycosidic bonds.[9] These bonds form long chains that contribute to its high tensile strength and rigidity.[10]

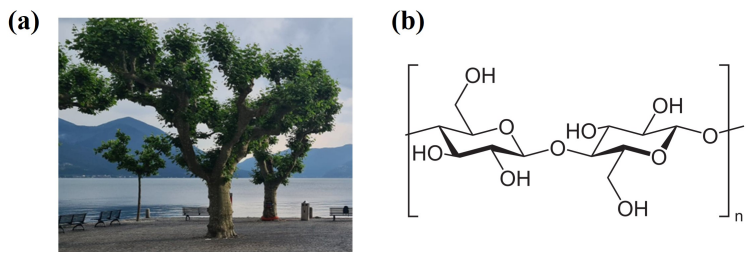

Figure 1.1. **(a)** Photograph of a tree, highlighting wood as a key example of cellulose's natural hierarchical organization. **(b)** Molecular structure of cellulose, depicting glucose monomers connected by β (1→4) glycosidic bonds.

When refined to the nanoscale, cellulose can transform into cellulose nanofibrils (CNFs), unlocking new possibilities in advanced materials design.[11]

1.2 Cellulose nanofibrils

Cellulose nanofibrils typically measure 5-60 nm in diameter with lengths of several micrometers.[12] Their high aspect ratio, mechanical strength, and versatile functional groups make them attractive for advanced materials. To produce CNFs with diameters of 2 to 10 nm, cellulose fibers are subjected to chemical pre-treatment and mechanical defibrillation.[13] This pre-treatment generates electrostatic repulsion and osmotic pressure, leading to the swelling of cellulose fibers in water. This process greatly enhances the efficiency of mechanical defibrillation, effectively breaking down fibril linkages to yield nanoscale cellulose fibrils. **Figure 1.2** displays an atomic force microscopy (AFM) image of typical cellulose nanofibrils.

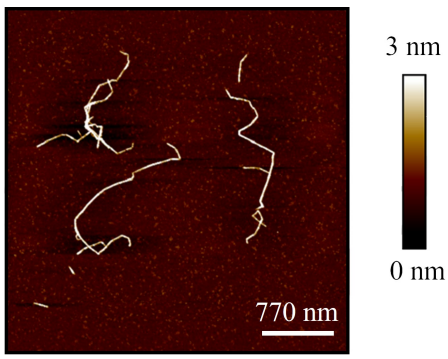

Figure 1.2. AFM image of TEMPO-oxidized cellulose nanofibrils, highlighting their nanoscale structure and high aspect ratio.

1.3 Stimuli-responsive materials

Stimuli-responsive materials are defined by their ability to respond to external triggers, such as temperature, pH, light, and voltage, leading to changes in their physical or chemical properties.[14] These adaptable materials have attracted significant interest across diverse fields. In biomedicine, for instance, pH-sensitive hydrogels enable targeted drug delivery by responding to specific physiological conditions.[15] In advanced robotics,[16] electroactive polymers mimic natural muscle movements.[17] This section explores two applications of stimuli-responsive materials: soft actuators, designed to produce motion in response to stimuli, and chemical sensors, carefully engineered for accurate environmental detection and measurement.

1.3.1 Soft actuators

Soft actuators are devices designed to produce motion in response to external stimuli.[18] Unlike traditional actuators with rigid moving parts, these devices utilize stimuli-responsive materials for motion generation.[19] Their flexibility, adaptability, and capability to mimic natural motions render them ideal for delicate applications that require a gentle touch.[20]

The actuation in soft actuators primarily arises from physicochemical transformations in the materials upon exposure to stimuli, including volumetric expansion,[21] and changes of molecular alignment.[22] Typically, it is the asymmetric manifestation of these changes that prompts actuation in the device.[23]

1.3.2 Chemical sensors

Stimuli-responsive sensors, distinct from actuators, are intricately designed to detect and measure specific environmental changes.[24] Within this category, chemical sensors form a specialized subset, adept at converting various chemical stimuli into quantifiable data.[25] For instance, CO_2 sensors are tailored to detect carbon dioxide levels,[26-28] while others are configured to sense volatile organic compounds,[29] or monitor changes in pH levels.[30] The design of these sensors typically involves materials that interact specifically with certain chemical substances, thereby enabling precise detection and measurement.

1.4 Literature survey and knowledge gaps

While the existing body of literature on cellulose-based stimuli-responsive materials,[31] especially in the field of cellulose actuators,[32] is extensive, there are several underexplored areas and challenges that this thesis aims to address.

1.4.1 Advancements in existing literature

Cellulose-based materials,[33] particularly cellulose nanofibrils, have been extensively researched for their potential in creating "smart" materials,[34] that are responsive to stimuli such as moisture,[35] pH,[36] and electric fields.[37] Their biocompatibility, biodegradability, and mechanical robustness position them as promising candidates for applications in soft robotics,[38] wearable technologies,[39] and biomedical devices.[40]

1.4.2 Identified knowledge gaps

- *Long-term stability and durability*: A significant gap in research is the limited understanding of the long-term stability and durability of cellulose-based actuators under continuous or repeated use. This is especially crucial for practical applications where reliability and longevity are paramount.

- *Scalability*: Another area requiring further exploration is the scalability of production methods. Most current studies and applications are confined to laboratory-scale demonstrations, with the transition to industrial-scale production remaining a challenge.

- *Cellulose nanofibrils-based sensors*: The development of CNFs-based sensors, particularly for environmental monitoring, is still in its infancy. While there have been some studies on using cellulose in sensors,[41,42] the potential for expansion is significant. Developing sensors capable of effectively and accurately detecting environmental changes could have substantial implications for environmental monitoring and protection.

1.4.3 Thesis objectives in addressing these gaps

This thesis aims to fill these gaps by:

- Exploring novel methods to enhance the scalability of CNFs-based actuators through techniques such as solvent casting, and investigate the durability.

- Investigating the potential of CNFs in response to less or unexplored stimuli, such as carbon dioxide, and for innovative applications such as environmental sensing and autonomous switching devices.

- Developing novel CNFs-based materials, including torsional and tensile actuators and capacitive sensors.

1.4.4 Structure and scope

The structure of this thesis is methodically delineated through well-defined stimuli, starting with moisture, then progressing to voltage, and ultimately CO_2 stimulus. Each section contributes to the existing body of knowledge and ventures into new domains of cellulose nanofibril applications. This approach effectively addresses the identified gaps and broadens the scope of research in cellulose-based stimuli-responsive materials.

1.5 Scope of the thesis

This thesis explores the response of cellulose nanofibrils-based materials to stimuli of interest (water, voltage, and CO_2) with the following objectives.

- To develop a variety of CNFs-derived, stimuli-responsive materials in different forms, including films, filaments, and foams, specifically for applications as soft actuators and sensors.

- To enhance the sensitivity of CNFs to the stimulus of interest through target synthesis and functionalization.

- To assess the performance of these materials by studying their properties and operational mechanisms.

- To demonstrate the practical applications of these CNFs-based materials *via* proof-of-concept demonstrations.

2. Preparation and Analysis of Materials

This chapter establishes the technical foundations for the development of cellulose nanofibrils-based materials and devices, which are further explored in subsequent chapters. It focuses on the detailed methods involved in the preparation and analysis of CNFs, outlining the essential steps from extraction and refinement to modification and characterization.

2.1 Synthesis of cellulose nanofibrils

The synthesized cellulose nanofibrils were derived from never-dried softwood kraft fiber pulp obtained from Norwegian spruce. The pulp consisted of 95% cellulose, 4.5% hemicellulose, and 0.1% lignin.

- For the negatively charged CNFs (**Figure 2.1a**), nanofibrils were obtained by subjecting the pulp to TEMPO-mediated oxidation, which introduced carboxylate groups onto the surface of the fibers. Subsequently, the oxidized fibers were mechanically defibrated to produce the cellulose nanofibrils material, as previously described by Saito *et al*.[43]

- For the positively charged CNFs (**Figure 2.1b**), the pulp underwent surface quaternization prior to mechanical treatment. This involved treating the pulp with sodium hydroxide and glycidyltrimethylammonium chloride, following a procedure outlined in the literature.[44]

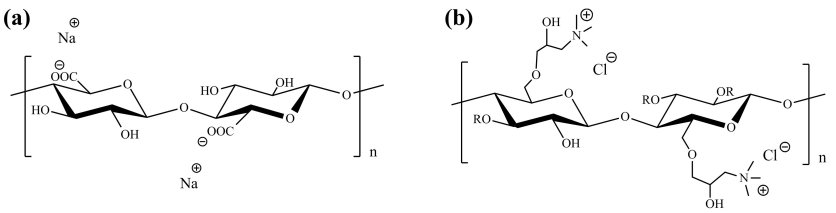

Figure 2.1. **(a)** Chemical structure of negatively charged cellulose nanofibrils, illustrating the characteristic hydroxyl and carboxylate groups introduced through the TEMPO-mediated oxidation process. **(b)** Chemical structure of surface-quaternized CNFs, highlighting the positively charged functional groups attached to the cellulose backbone.

2.2 Synthesis of graphene oxide

Graphene oxide (GO) was synthesized using the Hummers method.[45] In this process, graphite underwent a series of oxidation and exfoliation steps, involving a combination of sulfuric acid, sodium nitrate, and potassium permanganate. Following this, GO was isolated through multiple centrifugation washes, removing residual chemicals and by-products. The GO then underwent ultrasonication, which helped break down larger aggregates into finer flakes. This resulted in a stable, aqueous dispersion of GO, with individual flakes characterized by an approximate thickness of 1 nm (**Figure 2.2**).

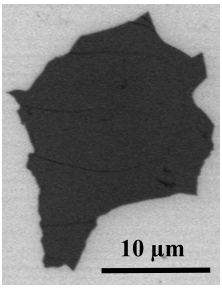

Figure 2.2. SEM image of monolayer graphene oxide (GO) flakes demonstrating the ultrathin profile of exfoliated GO. The flakes have an approximate thickness of 1 nm, achieved through the oxidation and ultrasonication processes used in the Hummers method. Adapted from Héraly *et al.* 2021.[46]

2.3 CNFs-based films, foams, and filaments

- Thin films of CNFs are fabricated using vacuum-assisted filtration through a PVDF membrane with an average pore size of 0.22 µm. A specified quantity of the CNFs dispersion, up to 0.1 wt%, is applied onto the membrane substrate. After filtration, the films are allowed to dry at room temperature for one hour. This drying period facilitates their easy detachment from the membrane substrate while preserving structural integrity.

- The fabrication process of CNFs-based foams begins with the transfer of a CNFs dispersion into a polypropylene beaker, which is then rapidly frozen using liquid nitrogen. Following this, the frozen sample is subjected to a freeze-drying process for a duration of 72 hours. This

extended period ensures the complete sublimation of ice, resulting in the formation of a porous foam structure.

- CNFs filaments are produced using a wet spinning process. Initially, a CNFs hydrogel, known as spinning dope, is extruded through a spinneret into an acetone coagulation bath, which leads to solvent exchange and transforms the hydrogel into a gel-thread. This thread then undergoes controlled drying under tension to form a dry filament.

2.4 Characterization techniques

Atomic force microscopy (AFM). A Multimode V instrument (Veeco) was used to acquire AFM images. The ScanAsyst air probe (Bruker) captured height, amplitude, and phase images in Peak Force tapping mode. Data analysis was conducted using NanoScope Analysis 1.5 software (Bruker).

ζ-Potential. The zeta potential of colloidal suspensions was measured using a Zetasizer analyzer (Malvern) at a temperature of 25°C and a pH level of 7. Each sample underwent three separate analyses to guarantee accuracy, thereby offering insights into the stability of the dispersions. High ζ-potential values suggest stable dispersions, attributable to the strong repulsive forces present between the particles.

Fourier transform infrared spectroscopy (FTIR). Infrared spectra were collected using an attenuated total reflectance Fourier-transform infrared (ATR-FTIR) spectrometer (Varian 610-IR), operating over a wavenumber range of 4000 to 400 cm^{-1}.

Powder X-ray diffraction (PXRD). A PANalytical X-ray system (X'Pert Pro) was used to record powder X-ray diffraction patterns, set at 40 mA and 45 kV, at 25°C, with a step size of 0.05°.

Tensile testing. Mechanical properties were assessed using an Instron 5960 dual column tabletop tensile testing machine. Samples were conditioned at a desired relative humidity and 22°C for 24 hours before testing. Data were processed using Bluehill Universal software (Instron).

Thermogravimetric analysis. A Discovery apparatus (TA Instruments) was used for thermogravimetric evaluation, heating materials from room temperature to 800 °C at a heating rate of 10°C/min in a nitrogen environment.

Gas sorption. Gas sorption properties of samples, for both nitrogen (N_2) and carbon dioxide (CO_2), were investigated using an ASAP2020 instrument (Micromeritics). The process started with degassing the samples at 80 °C for 10 hours under vacuum to remove pre-adsorbed gases or moisture. After degassing, N_2 adsorption at 77 K was carried out, allowing for the determination of surface area and pore size using the Brunauer-Emmett-Teller (BET) model,[47] and a Density Functional Theory (DFT) model,[48] respectively. Independently, CO_2 adsorption was also assessed at 273.15 K. During both N_2 and CO_2 adsorption measurements, quasi-equilibrium is achieved when pressure variation remains below 0.01% for at least 15 seconds.

Rheological measurements. A MCR 301 rheometer (Anton Paar) was utilized for the rheological characterization of the hydrogel. The analysis encompassed oscillatory shear tests, which were conducted to ascertain the storage (G') and loss (G") moduli, alongside steady shear tests aimed at measuring viscosity.

Scanning electron microscopy. A JSM-7000F machine (JEOL) was employed for SEM analysis. An acceleration voltage ranging from 1 to 15 kV was employed to create detailed images and analyze the chemical composition, benefiting from the ability to perform chemical analysis with an EDX detector.

Surface charge determination. Conductometric titration was used to assess the density of charged surface groups on cellulose nanofibrils.

3. Paper I & Paper IV: Moisture Stimulus

This chapter investigates the moisture-responsive properties of cellulose nanofibrils-containing films and fibers, highlighting how their inherent characteristics can be effectively utilized in developing soft actuators.[49-51] Emphasis is placed on the creation of various types of actuators, including bilayer, torsional, and tensile actuators, showcasing the versatility and potential applications of CNFs in response to moisture stimuli.[52]

3.1 Introduction

The discussion commences with an exploration of bilayer actuators, featuring an innovative design that combines negatively charged CNFs with reduced graphene oxide (rGO).[46] This configuration adapts effectively to humidity variations. The section further delves into how the cation exchange process can influence the performance of these actuators.

The study then shifts its focus to torsional actuators,[53] emphasizing the role of CNFs in creating strong, moisture-responsive filaments through wet-spinning techniques.[54] Subsequent twisting results in actuators capable of effective torsional motion in response to water vapor.

Lastly, the potential applications for tensile actuators[55] are explored, showcasing the innovative integration of CNFs with nylon filament cores for moisture-responsive core-sheath fibrous actuations.

3.2 Paper I: Bilayer actuator

Bilayer actuators,[56] composed of two layers of distinct materials engineered for differential response to external stimuli, exhibit asymmetric behavior.

The research focuses on a humidity-sensitive actuator, consisting of a CNFs layer and a rGO layer, which collectively demonstrate exceptional humidity-responsive behaviors.

3.2.1 Fabrication method

The bilayer actuator comprises one layer of TEMPO-oxidized cellulose nanofibrils (TCNFs-Na^+) and an adjacent layer of rGO sheets. The fabrication process of the bilayer actuator is depicted in **Figure 3.1**. A film was formed by vacuum-filtering a TCNFs-Na^+ aqueous dispersion onto a PVDF membrane substrate. Following this, an aqueous GO dispersion was added onto the wet film and vacuum-filtered to create a bilayer, which was then peeled off and treated by hydrogen iodide (HI) vapor to reduce GO, thereby imparting hydrophobic and graphene-like properties to the GO sheets.

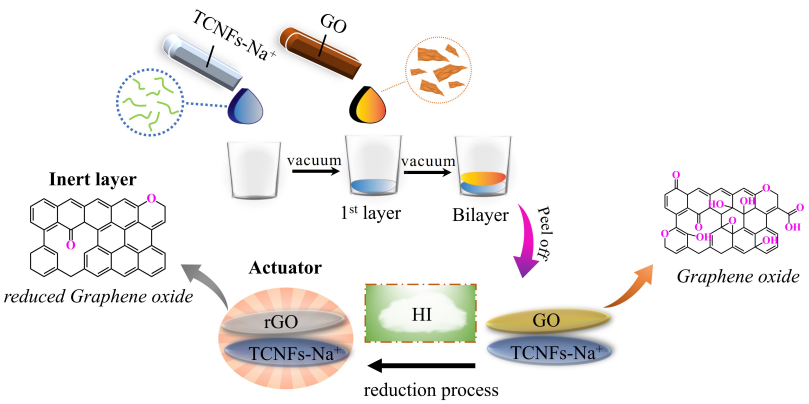

Figure 3.1. Illustration of the bilayer actuator assembly. Adapted from Héraly *et al*. 2021.[46]

In total, six bilayer actuators were constructed. Each with varying thicknesses of the CNFs layer ranging from 0.12 µm to 4.18 µm, and a constant thickness of the rGO layer maintained at 0.40 µm. These bilayer actuators, designated as TCNFs-Na^+_y/rGO, where ***y*** denotes the thickness of the CNFs layer, were then cut into strips measuring 5 mm × 1 mm for performance evaluation.

3.2.2 Analysis of operational mechanisms

When exposed to different humidity levels, the actuator demonstrates a prompt and significant movement driven by humidity changes. As relative humidity (RH) increases, the CNFs layer undergoes expansion by absorbing moisture, as illustrated in **Figure 3.2a**. By contrast, the rGO layer remains relatively unaffected by humidity changes. This asymmetry in response between the two layers results in the bending of the actuator (**Scheme 3.1**). Correspondingly, a decrease in RH leads to water desorption from the CNFs layer, causing the actuator to return to an unbent state.

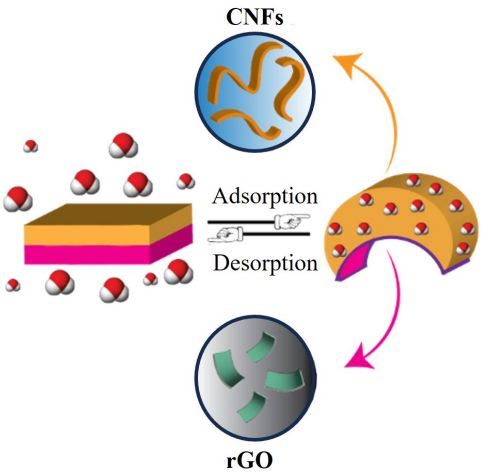

Scheme 3.1. Schematic depiction of the actuation mechanism. This diagram illustrates the asymmetric volume expansion induced by water sorption, which leads to a bending motion, followed by volume contraction resulting from water desorption, culminating in an unbending state.

Mechanical studies of the TCNFs-$Na^{+}_{0.37\mu m}$ film reveal significant variations in its properties under different RH conditions (**Figure 3.2b**). At a low RH of 25%, the film exhibits excellent strength and stiffness, with a recorded tensile strength of 156.7 MPa and a Young's modulus of 13.7 GPa, along with a strain at break of 1.1%. In parallel, at a high RH of 95%, the film undergoes substantial softening, leading to drastic reduction in its mechanical properties. The tensile strength decreases to 15.3 MPa, and the Young's modulus drops to 0.56 GPa. These changes can be attributed to the swelling of the CNFs layer due to uptake of moisture.

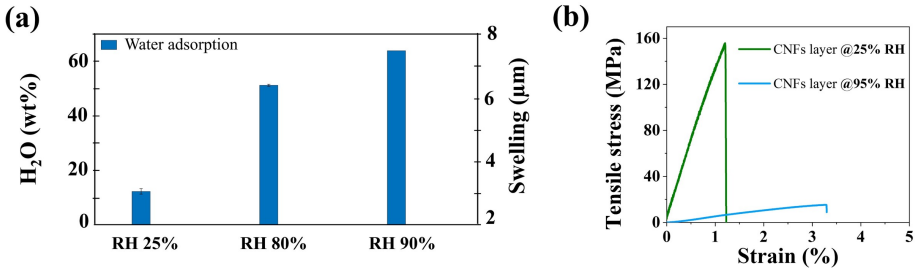

Figure 3.2. **(a)** Water uptake and swelling of the CNFs layer in response to increased relative humidity. **(b)** Stress–strain curves of the pristine TCNFs-$Na^{+}_{0.37\mu m}$ film, highlighting its excellent strength and stiffness at 25% RH, as well as the pronounced reduction in mechanical properties observed at 95% RH for the same film due to softening and swelling. Adapted from Héraly *et al*. 2021.[46]

The bending motion of the actuator, resulting from these mechanical changes, is analyzed through curvature calculations, as illustrated in **Figure 3.3**.

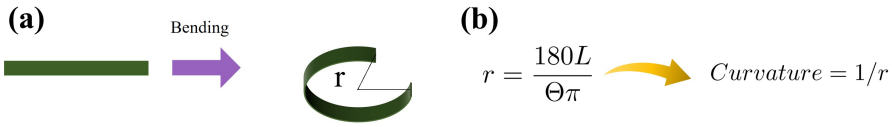

Figure 3.3. **(a)** An illustration depicting the bending motion of the actuator. **(b)** The relationship between curvature and the free length (L), radius (r), and central angle (θ) of the actuator. Adapted from Héraly *et al*. 2021.[46]

In summary, the performance of the actuator is inherently connected to the mechanical properties of the CNFs film, which exhibit significant variations in response to changes in RH.

3.2.3 Performance

The actuator's effectiveness is determined by the thickness of the CNFs layer. At a thickness of 0.12 µm, TCNFs-Na^+/rGO showed minimal actuation (**Figure 3.4a**). By contrast, the TCNFs-$Na^+_{\mathbf{0.37\mu m}}$/rGO version demonstrated excellent performance in terms of both curvature and response speed, making it the optimal choice (**Figure 3.4a-b**). This model achieved a 360º bending in 8.8 seconds when RH shifted from 25% to 95% and then returned to an unbent state in just 0.92 seconds as RH was reverted to 25% (**Figure 3.4b**).

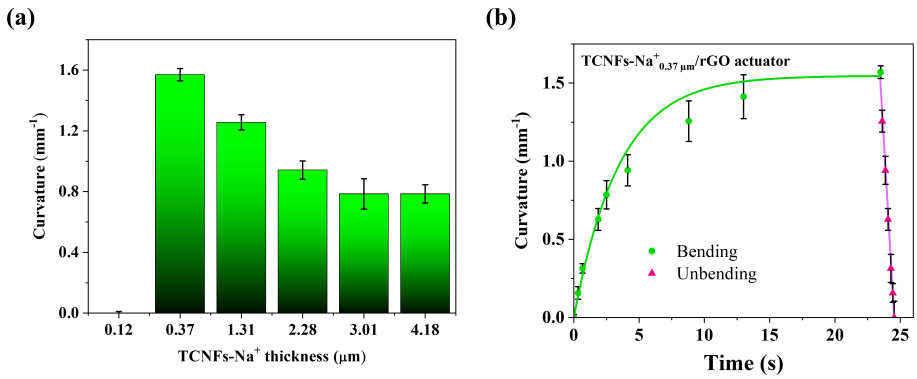

Figure 3.4. **(a)** The relationship between the curvature and the thickness of the TCNFs-Na^+ layer in the actuators, with the rGO layer held constant at 0.40 µm; tests were conducted as RH shifted from 25% to 95%. **(b)** Bending kinetics of the optimized TCNFs-$Na^+_{\mathbf{0.37\mu m}}$/rGO bilayer actuator as RH varied from 25% to 95% and then returned to 25%. Adapted from Héraly *et al*. 2021.[46]

After 100 cycles, the actuator's performance slightly declined, with the bending curvature reducing from 1.57 mm^{-1} in the 1st cycle to 1.41 mm^{-1} in the 100^{th} cycle (**Figure 3.5**). This 10.7% decrease, exceeding a 5% threshold for statistical significance, indicates a notable degradation in performance over time, likely due to residual moisture in the CNFs layer.

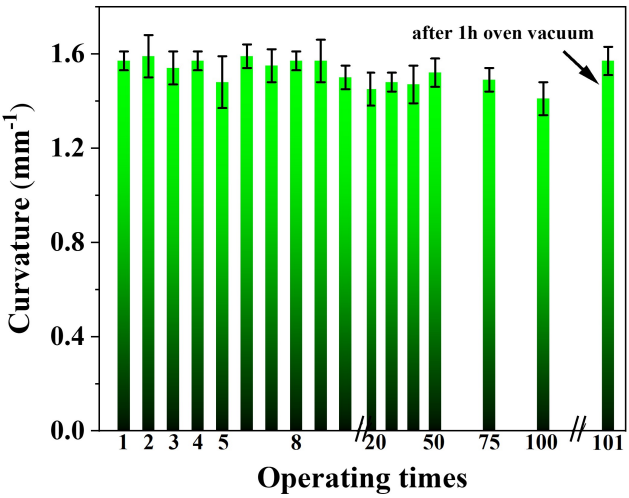

Figure 3.5. This graph illustrates the maximum bending curvature of TCNFs-$Na^{+}_{0.37\mu m}$/rGO over 100 cycles of repeated actuation between 25% and 95% RH, highlighting a slight performance decrease due to residual moisture trapped in the CNFs layer. The actuator's initial performance was restored in the 101st cycle following a vacuum treatment to remove residual moisture. Adapted from Héraly *et al*. 2021.[46]

3.2.4 Cation control

Multiple TCNFs-$Na^{+}_{0.37\mu m}$/rGO actuators were fabricated, and cation exchange experiments were conducted with the goal of modulating the moisture interaction behavior of the actuator to tune its actuation performance. By substituting sodium countercations with proton (H^{+}) or tetraalkylammonium cations such as tetraethylammonium (TEA^{+}), tetrabutylammonium (TBA^{+}), and tetrahexylammonium (THA^{+}), the potential for actuation control was explored.

The hypothesis was that longer hydrophobic alkyl tails in ammonium cations would reduce the layer's moisture interaction. Experimental results validated this hypothesis, revealing a decrease in actuation performance with longer alkyl chain lengths. The TCNFs-$THA^{+}_{0.37\mu m}$/rGO actuator, in particular, exhibited little-to-no observable actuation (**Figure 3.6**).

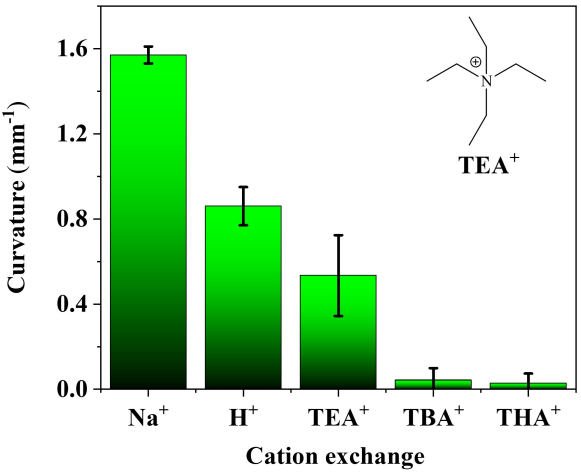

Figure 3.6. Influence of countercations on actuation curvature, demonstrating their impact on the maximum curvature of the actuator. The inset provides the chemical structure of a representative cation tetraethylammonium. Adapted from Héraly et al. 2021.[46]

3.2.5 Autonomous oscillation of TCNFs-$Na^{+}_{0.37\mu m}$/rGO actuator in high humidity environment

In a proof-of-concept application, as illustrated in **Figure 3.7**, the TCNFs-$Na^{+}_{0.37\mu m}$/rGO actuator was integrated into an autonomous, self-oscillating circuit within a high humidity chamber, Within this system, the actuator serves as a dynamic switch, bending in response to the elevated humidity level (RH = 92%), and establishing contact with a copper plate to close the electrical circuit and illuminate a lamp.

The resulting current flow induces Joule heating in the rGO film that warms up the nearby TCNFs-Na^{+} layer, leading to water evaporation from the TCNFs-Na^{+} layer. This evaporation causes the actuator to unbend, interrupting the circuit and canceling the Joule heating. As the rGO cools down, the TCNFs-Na^{+} layer reabsorbs moisture, triggering a new bending-unbending cycle.

This proof of concept highlights the significant potential of these actuators in developing systems capable of autonomously adapting to environmental changes, eliminating the need for external intervention.

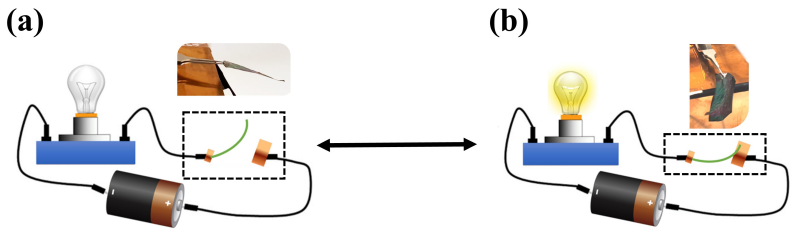

Figure 3.7. A schematic illustrating an autonomous, self-oscillating electrical circuit featuring a bilayer actuator within a humidity chamber set to 92% RH. The cycle begins with the actuator bending in response to the high RH, closing the circuit through the rGO layer **(b)**, which allows electron flow and activates a light. Subsequently, Joule heating, generated by the current, elevates the temperature of the rGO layer, leading to water desorption from the TCNFs-Na^+ layer and causing the actuator to unbend, returning to its original state **(a)**. This process repeats autonomously in the humidity chamber, forming a self-sustaining cycle without the need for external energy input. Adapted from Héraly *et al*. 2021.[46]

3.3 Paper IV: Torsional actuator

This section outlines the transformation of the cellulose nanofibrils-derived filament into a water-responsive torsional actuator, a device designed to produce rotational motion in response to moisture.[57]

3.3.1 CNFs filament production

The development of a torsional actuator utilizing CNFs hinges on the wet spinning process. This technique involves extruding a CNFs-based spinning dope through a spinneret into a coagulation bath. The process results in the formation of a gel-thread, which eventually dries to become a robust filament.

Central to this process is the choice of coagulation bath. Acetone is selected for its rapid solvent exchange capability with water and its low boiling point. When the spinning dope is introduced into the acetone bath, it undergoes a swift exchange of water with acetone, leading to quick coagulation. This is critical because acetone's lower polarity than water reduces hydrogen bonds with the CNFs, causing them to aggregate and form a densely packed gel-thread. This method also eliminates the need for subsequent washing processes often required with other solution such as aqueous HCl.

Transitioning to gel-thread formation, achieving high alignment of CNFs during this phase is crucial for the optimal mechanical properties of the filaments later on. In this goal, the concentration of the spinning dope plays a significant role. High CNFs concentrations can hinder alignment of nanofibrils during shear flow, whereas low concentrations lead to predominant Brownian motion, negatively impacting alignment and the strength of the gel-thread. To counteract these effects, the dope concentration is maintained at 0.7 wt%, and the extrusion rate is carefully optimized to be 0.3 ml/min which is the rate experimentally determined to be the most effective for proper nanofibril alignment under shear flow.

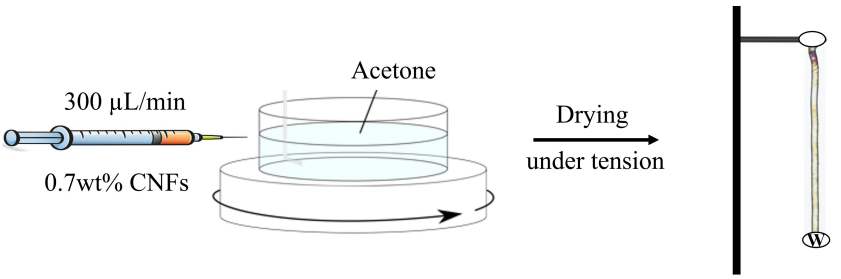

Scheme 3.2. A schematic illustrating the setup used for wet spinning to obtain a CNFs gel-thread in the coagulation bath which is then lift up and dry under a 0.5g small tension load (W) to minimize shrinkage and deformation and yield a CNFs filament.

Incorporating a small amount of microcellulose fibers (MFCs) into the spinning dope is needed as it significantly enhances the final filament's strength. The dimensionally larger MFCs effectively intertwine with the nanofibrils, reinforcing the gel-thread's structural integrity during the coagulation phase and reducing the likelihood of breakage.

The optimized filament, labeled as Opti-CNFs, formulated with a 9:1 dry weight ratio of CNFs to MFCs, showcases enhanced mechanical properties when compared to both pristine CNFs filaments and those with an equal CNFs to MFCs mass ratio, referred to as Half-CNFs (**Figure 3.8a**). This optimized ratio effectively balances the robustness provided by MFCs with the unique properties of CNFs. However, an excess of MFCs in the filament can disrupt this balance, leading to mechanically weaker filaments (**Figure 3.8b**). Such imbalance also hinders the preservation of the nano-scale structure of CNFs, which is crucial for maintaining inherent qualities such as increased surface area and enhanced sensitivity to moisture.

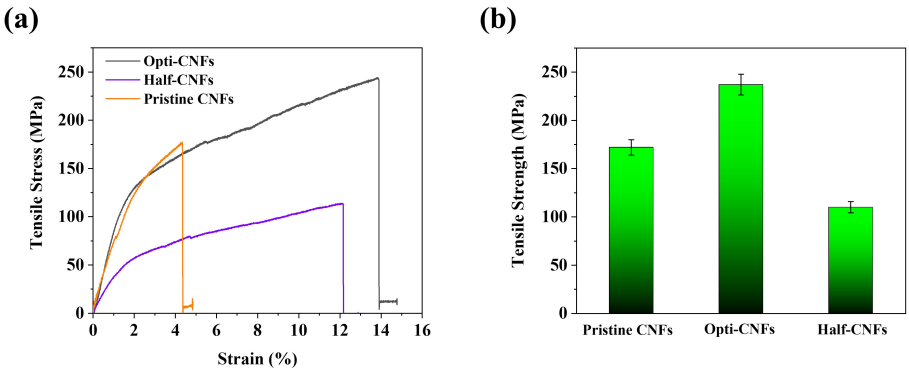

Figure 3.8. (a) Tensile stress-strain relationships for Opti-CNFs filaments, Half-CNFs, and pristine CNFs filaments, highlighting the pronounced effect of spinning dope formulation on the mechanical properties of each filament type. **(b)** Comparative analysis of the maximum tensile strength observed in the three types of filaments.

The rheological behavior of the Opti-CNFs spinning dope is depicted in **Figure 3.9a**. Additionally, **Figure 3.9b** provides detailed SEM images of the Opti-CNFs filament, revealing both its surface morphology and cross-sectional structure.

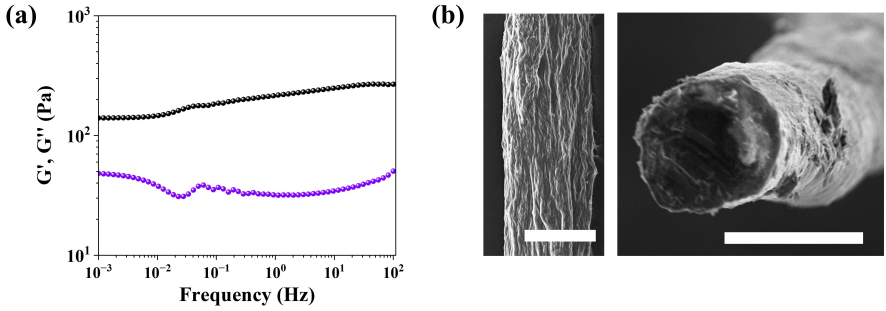

Figure 3.9. **(a)** Rheological behavior of the Opti-CNFs spinning dope as a function of frequency. **(b)** SEM image showing the surface morphology and cross-sectional structure of the Opti-CNFs filament (Scale bar, 100 µm).

3.3.2 Initiation of twisting in the Opti-CNFs filament

After acquiring the Opti-CNFs filament, its twisting phase is initiated by suspending it between a rotational motor, with a tension of 1.0 MPa applied. A rotational speed of 85 rpm is set, allowing only free longitudinal movement to effectively insert twists into it. This process, lasting for 4 minutes, introduces a twist density of 2500 turns per meter and a measured bias angle (α) of 41° relative to the filament's axial direction (Figure 3.10).

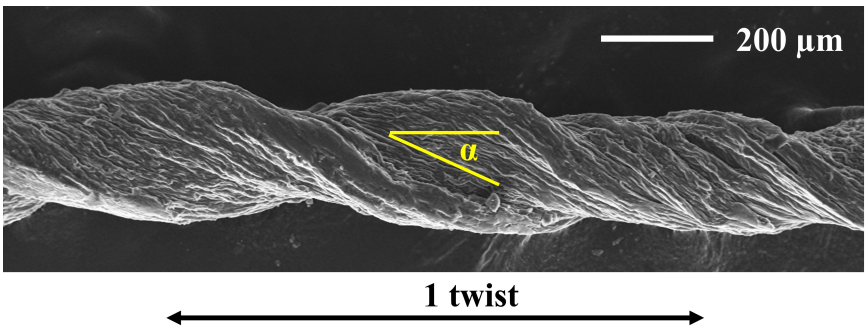

Figure 3.10. SEM image of the torsional actuator, displaying its twisted structure characterized by a significant 41° bias angle (α). For reference, a complete twist is defined as 360° rotation.

3.3.3 Actuation mechanism and performance

A CNFs-based torsional actuator, designed for rotational motion in response to moisture, swells upon exposure to water vapor. The swelling, a result of the hydrophilic nature of CNFs, is more pronounced radially than axially due to the helical structure of the CNFs. This asymmetric volume increase leads to partial untwisting of the actuator and shortening due to internal mechanical stresses arising from the anisotropic expansion. The untwisting alters the helix diameter, generating torque and initiating torsional rotation. Upon water desorption, as the CNFs release the absorbed water and shrink back, both the generated torque and internal stresses decrease. This process reverses the rotation direction, eventually restoring the actuator to its original state (**Figure 3.11a**).

The experimental data provided further insights into the actuator's behavior. When subjected to water vapors for 20 seconds, the actuator commenced rotation, peaking at an acceleration of 2000 rad/s^2 after 3.8 seconds and reaching

a maximum rotational speed of 1180 rpm within 10 seconds. However, this dynamic response was not sustained indefinitely; after 18.7 seconds, as it approached water capture saturation, the actuator began to decelerate, halting completely at the end of water exposure (**Figure 3.11b-c**).

To assess durability, the actuator underwent a series of tests involving repeated 20-second exposures to water vapors, each followed by a 15-minute resting period. Initially, it maintained high rotational speeds for the first five cycles, demonstrating resilience (**Figure 3.11d**). However, continued exposure over 30 cycles revealed a decline in performance, evidenced by a 50% decrease in maximum rotational speed.

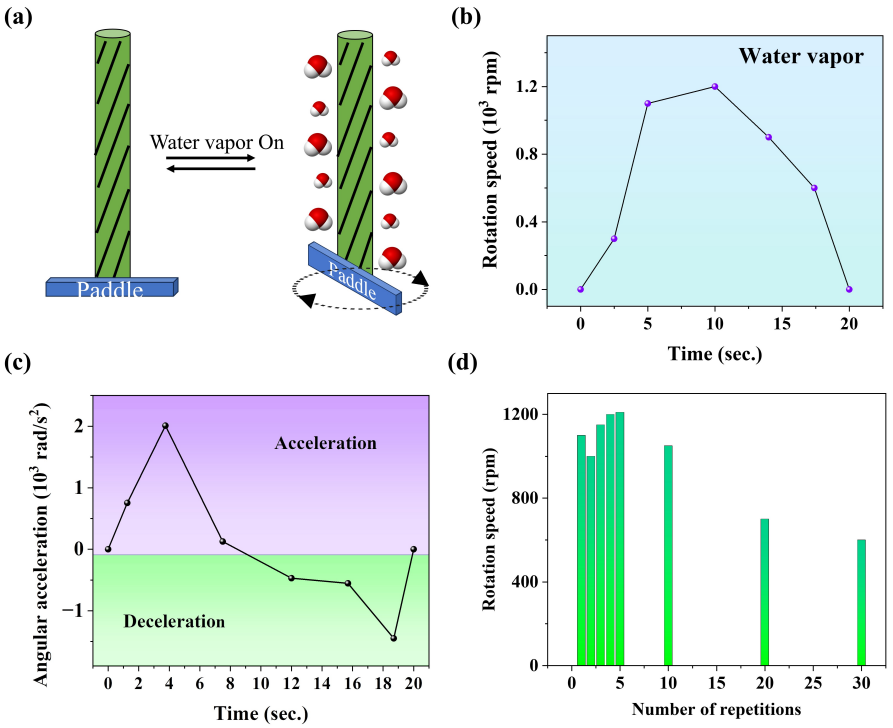

Figure 3.11. (a) Schematic of the actuation mechanism illustrating a paddle that exhibits rotational motion upon exposure to water vapors. **(b)** Graph depicting the kinetics of rotational speed for the CNFs-based torsional actuator, reaching a peak speed of 1180 rpm after 10 seconds. **(c)** Kinetics of angular acceleration, with a peak acceleration of 2000 rad/s^2 achieved after 3.8 seconds. **(d)** Durability test results after 30 cycles, indicating a 50% decrease in rotational speed, likely caused by residual moisture retention and material fatigue in the torsional actuator.

3.4 Paper IV: Tensile actuator

A CNFs-based tensile actuator is designed for linear motion in response to moisture. This work introduces an innovative configuration that combines a robust nylon core with a moisture-sensitive CNFs sheath. This synergistic combination of the nylon core and the CNFs sheath enhances adaptability and responsiveness, making it ideal for a variety of "smart" materials applications.

The fabrication process begins with a nylon fiber as the core, having an initial diameter of (282 ± 2) µm (**Figure 3.12a**). This core is subjected to a coiling process through twisting, followed by a sequential two-stage thermal setting to result in a supercoiled structure, enlarging its diameter to (660 ± 4) µm as confirmed by SEM (**Figure 3.12b**).

Following this, the supercoiled nylon undergoes a triple-coating in a 0.75 wt% CNFs dispersion. This coating process results in a (260 ± 7) µm thick CNFs sheath. This sheath configuration significantly enhances the moisture sensitivity of the actuator (**Figure 3.12c**).

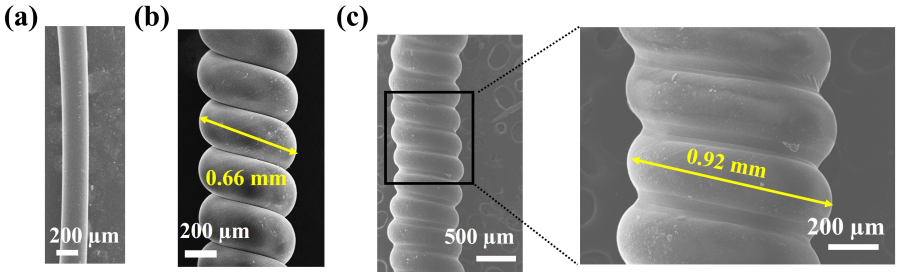

Figure 3.12. Sequential steps for creating the sheath-run tensile actuator. **(a)** Starting with a nylon fiber as the core of 282 µm in diameter. **(b)** Coiling and thermally setting it. **(c)** Applying the CNFs sheath *via* dip-coating method, resulting in a total actuator thickness of 920 µm.

The actuation mechanism of this tensile actuator relies on the interplay between the inherent torque of the supercoiled nylon and the CNFs material. The spring-like nylon core stores significant torque, while the CNFs sheath swells upon moisture exposure, generating external torque. This combination of torques results in linear contraction of the actuator. When moisture is desorbed, the external torque diminishes, enabling the actuator to revert to its original state.

The effectiveness of the tensile actuation is significantly influenced by the sheath-to-core ratio, with previous studies suggesting an optimal ratio of 0.3 for the maximum efficiency.[58] A sheath that is excessively thick might impede contraction, whereas a sheath that is too thin may not offer sufficient responsiveness toward moisture. In the fabrication process described, an optimal sheath-to-core ratio of 0.4 has been achieved.

3.5 Perspective

The groundbreaking development of CNFs-based actuators, including bilayer, torsional, and tensile types, heralds a new era in moisture-responsive actuation technology. These actuators, leveraging the hydrophilicity and mechanical robustness of CNFs, have demonstrated immense potential across various applications, dynamically responding to environmental changes. While significant progress has been made, future efforts will be directed toward more comprehensive actuation tests to reveal the structure-property-function relationship.

4. Paper II: Voltage Stimulus

Voltage stimulus is essential in applications that demand precise responsiveness and flexibility, such as artificial muscles and soft robotics.[59] This chapter explores the adaptability of CNFs and the significant role of electrolytes and counteranions in their functions. It also broadens our understanding of CNFs capabilities, moving beyond just moisture sensitivity.

4.1 Introduction

Electro-actuators based on CNFs are part of the family of actuators derived from ionic electro-active polymers (iEAPs).[60] These materials are capable of converting electrical signals into physical movement.[61] This conversion is achieved primarily through ion migration, a process effectively facilitated at low voltages ($\leq$ 5V).[62]

Building on this, the choice of electrolyte type, in conjunction with the effect of various anions on actuation,[63] plays a pivotal role in dictating the performance of these CNFs-based actuators. Therefore, a comprehensive understanding of these factors is key to optimizing both the efficiency and responsiveness of the actuators.

The surface chemistry of CNFs can be specifically tailored to interact more strongly with certain desired anions, enabling precise tuning of physicochemical properties.[64] Additionally, due to their impressive mechanical strength,[65] CNFs processed into films serve as the mechanical matrix of the as-constructed electro-actuator.

4.2 Role of electrolytes and counteranions

The objective of this study is to explore how different types of electrolytes and ions can improve the performance and versatility of CNFs-based electro-actuators. This research focuses on two main series of electrolytes: lithium (Li)-based salts and imidazolium-based ionic liquids (as depicted in **Figure 4.1**).[66] Li-based salts are favored for their rapid ion diffusion,[67] which is ideal for high-speed actuation applications. By contrast, imidazolium alternatives stand out due to their broad electrochemical windows,[68] and features such as low vapor pressure,[69] excellent thermal stability,[70] and high ionic conductivity.[71]

Additionally, the influence of specific anions on the electro-actuator's performance is thoroughly investigated. Anions of interest include chloride (Cl^-), tetrafluoroborate (BF_4^-), bis(trifluoromethane sulfonyl)imide ($TFSI^-$), and hexafluorophosphate (PF_6^-). Their sizes are shown in **Table 4.1**.

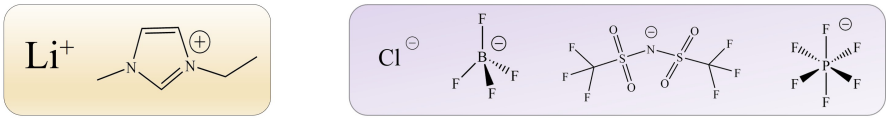

Figure 4.1. Chemical structures of the cations and anions used in this study.

Table 4.1. Van der Waals volume of the investigated ions.[72,73]

Ions	Van der Waals volume ($Å^3$)
BF_4^-	48
$TFSI^-$	189
PF_6^-	68
Cl^-	24.8
Li^+	1.84
$EMIM^+$	118

4.3 Fabrication of the CNFs-based electro-actuators

The fabrication process of the electro-actuator begins with a dispersion of positively charged CNFs containing chloride as the natural counteranion, which can undergo an anion exchange process by reaction with an excess of the selected electrolyte. The procedure involves multiple solvent-exchange steps, leading to the formation of a CNFs-X dispersion in methanol, where ***X*** denotes the counteranion such as BF_4^-, PF_6^-, or $TFSI^-$. This dispersion is then carefully combined with a corresponding electrolyte, such as LiTFSI or $EMIMPF_6$, to achieve a 1:1 dry weight ratio of electrolytes to CNFs. Following this, the solution casting technique is employed to produce the composite films, designated as CNFs-X@LiX or CNFs-X@EMIMX. The final step in the fabrication process involves the deposition of an ultrathin gold layer as current collector using sputtering techniques onto both surfaces of these films, as illustrated in **Figure 4.2**.

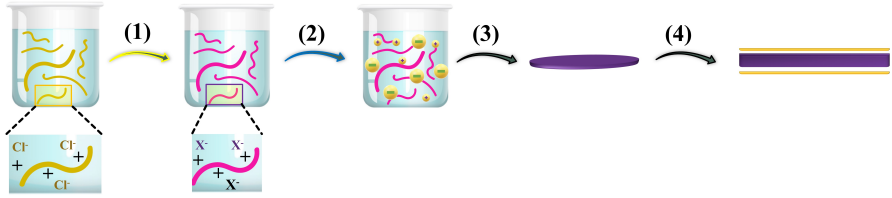

Figure 4.2. Illustration of the fabrication steps of CNFs-based electro-actuators. **(1)** Anion exchange process of CNFs-Cl, where chloride ions are replaced by alternative anions; **(2)** Integration of electrolyte into the CNFs-X dispersion, **(3)** Film formation *via* a solution casting method; **(4)** Gold sputtering on both surfaces of the film. Remodeled from Héraly et al. 2023.[66]

In our investigation of the structural characteristics of CNFs-based actuators, the detailed architecture plays a pivotal role in their functional performance. Figure 4.3 presents a SEM cross-sectional view of the CNFs-TFSI@LiTFSI actuator. This image reveals the intricate layering within the actuator, including the thin two gold electrode layers on the top and at the bottom, and the overall thickness of the CNFs composite film.

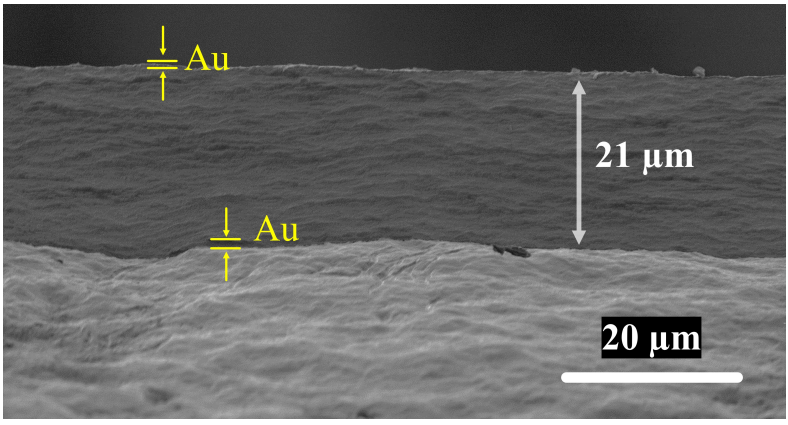

Figure 4.3. SEM cross-sectional view of the CNFs-TFSI@LiTFSI actuator as an example. This cross-section showcases the two very thin gold electrode layers that sandwich the CNFs composite film with a thickness of 21 µm. Remodeled from Héraly et al. 2023.[66]

4.4 Actuator's response to voltage stimulus

When a voltage is applied to CNFs-based electro-actuators, both cations and anions are set in motion. Specifically, cations move toward the cathode (the negatively charged electrode), while anions migrate toward the anode (the positively charged electrode). This ion movement leads to an asymmetric volume expansion of the cathode and anode area, visually depicted in Figure 4.4**a**, which in turn drives the actuation process if the volume variation on two electrodes is different. The degree of this bending action is quantifiable, and its magnitude can be determined by analyzing the bending strain, as detailed in Figure 4.4**b**.

In this context, if not specified, “bending inward” refers to the actuator's curvature moving toward the cathode side, while “bending outward” indicates curvature moving away from the cathode side. This means that bending outward is equivalent to bending inward relative to the anode. These terms are consistently used throughout our study to describe the actuator's movement in relation to the cathode.

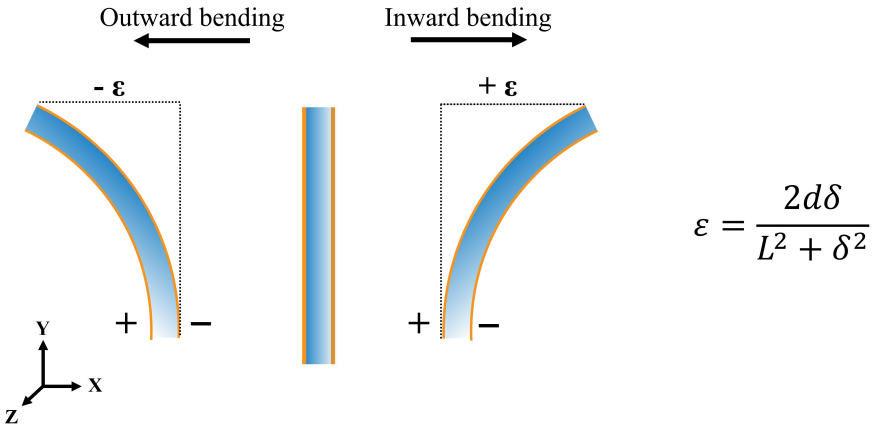

Figure 4.4. Illustration of the bending motion resulting from the voltage-induced asymmetric volume expansion in CNFs-based electro-actuators. Included is a formula for calculating bending strain, ε, where d represents the width of the actuator, L signifies its unconstrained length, and δ measures the lateral bending displacement in the X-direction.

4.5 Performance analysis

4.5.1 Li-based salt series

In the Li-based salt series, the CNFs-TFSI@LiTFSI electro-actuator outperformed the others, delivering the highest bending strain (**Table 4.2**). By contrast, CNFs-Cl@LiCl exhibited no actuation. This absence of bending is attributed to the limitations of the chloride anion under applied voltage, potentially leading to its decomposition. Additionally, the small size of the chloride ion results in a negligible contribution to actuation, rather than being due to strong ionic interactions within the matrix.

Table 4.2. Maximum bending strain (in absolute values) for each CNFs-X@LiX actuator under 3.0 V DC and 5.0 V DC.

	ε (%)	
Actuators	**3.0V**	**5.0V**
CNFs-Cl@LiCl	0	0
CNFs-BF_4@LiBF_4	0.0083	0.027
CNFs-TFSI@LiTFSI	0.111	0.108
CNFs-PF_6@LiPF_6	0.0735	0.1

The plasticization effect plays a critical role in this series. Among the four anions studied (BF_4^-, Cl^-, $TFSI^-$, and PF_6^-), the $TFSI^-$ anion, due to its significantly large size (*Van der Waals* volume of 189 $Å^3$)[72] and partially delocalized charge, more strongly plasticizes the CNFs matrix. This results in a more amorphous structure, as shown in Figure 4.5**a**. It also alters the mechanical properties of the composite film (Figure 4.5**b**) and enhances the mobility of ions within the CNFs matrix by forming weaker interactions with them.

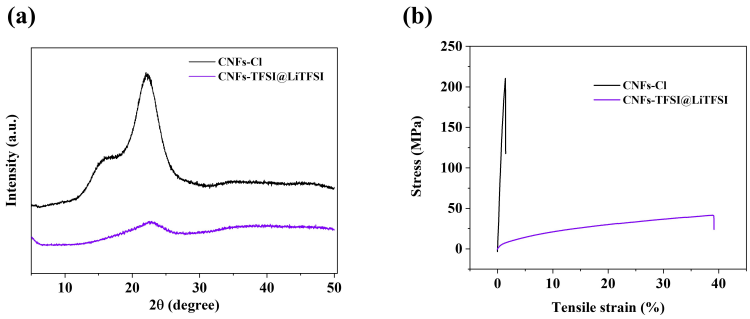

Figure 4.5. (a) PXRD patterns of both the CNFs-Cl film and the CNFs-TFSI@LiTFSI film. **(b)** Tensile test results for the CNFs-TFSI@LiTFSI film in comparison to the pristine CNFs-Cl film. Remodeled from Héraly et al. 2023.[66]

Thanks to its plasticization effect and large size, $TFSI^-$ anions migrate toward the anode, leading to differential volume expansion at the anode *i.e.* the volume expansion at the anode is much larger than that at the cathode. This uneven expansion causes the actuator film to bend, with the cathode side curving inward. The actuation kinetics of the CNFs-TFSI@LiTFSI actuator under two voltages, 3.0 V and 5.0 V DC, are shown in **Figure 4.6a**. The kinetic behavior follows a logarithmic curve and exhibits a discernible plateau after approximately 500 seconds for both excitation voltages. The inward bending to cathode at 3V and 5V is illustrated in **Figure 4.6b,** while its response under a 3.0 V AC square wave at 0.01 Hz, which outperforms the others, is depicted in **Figure 4.6c**.

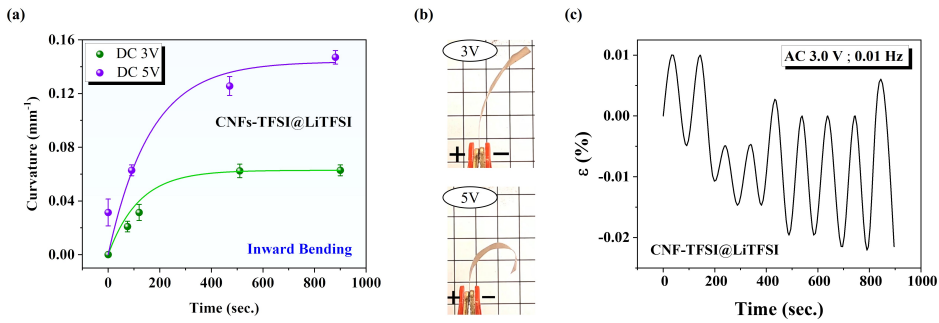

Figure 4.6. **(a, b)** Kinetics of the CNFs-TFSI@LiTFSI actuator's inward bending to cathode when subjected to 3.0 V DC (green line) and 5.0 V DC (magenta line), showing the logarithmic kinetic curve with a plateau phase after approximately 500 seconds. **(c)** Depiction of the actuator's response under a 3.0 V AC square wave at 0.01 Hz. Remodeled from Héraly et al. 2023.[66]

4.5.2 EMIM-based electrolyte series

Ion mobility significantly influences the behavior of EMIM-based CNFs electro-actuators. Under a 3.0 V DC, CNFs-Cl@EMIMCl, such as CNFs-Cl@LiCl, exhibits no actuation due to the same underlying reasons. By contrast, CNFs-TFSI@EMIMTFSI and CNFs-BF_4@EMIMBF_4 actuators exhibit inward bending, hypothesized to be due to the limited solubilization of $EMIM^+$ cations in the positively charged CNFs matrix, creating an energetic barrier to their movement. This results in asymmetric volume expansion, predominantly on the anode side, leading to the inward bending of the actuator. These observations are quantitatively supported by the data shown in **Table 4.3**, which presents the maximum bending strain in absolute values for each CNFs-X@EMIMX actuator under 3.0 V DC and 5.0 V DC.

Table 4.3. Maximum bending strain in absolute values for each CNFs-X@EMIMX actuators under a 3.0 V DC and 5.0 V DC**.**

	ε (%)	
Actuators	**3.0V**	**5.0V**
CNFs-Cl@EMIMCl	0	0
CNFs-BF_4@EMIMBF_4	0.038	0.111
CNFs-TFSI@EMIMTFSI	0.0739	0.151
CNFs-PF_6@EMIMPF_6	0.0304	0.111

The larger $TFSI^-$ anion in the CNFs-TFSI@EMIMTFSI actuator results in a more pronounced bending strain and better curvature kinetic over time (**Figure 4.7a**) than the CNFs-BF_4@EMIMBF_4 actuator.

At 5V, both CNFs-TFSI@EMIMTFSI and CNFs-BF_4@EMIMBF_4 actuators initially bend inward, then after some time, outward, as shown in **Figure 4.7b**. This sequence suggests that $EMIM^+$ cations, after initially facing resistance, overcome the energetic barrier of the cationic CNFs matrix and migrate toward the cathode, resulting in significant volume expansion on this side. Specifically for CNFs-TFSI@EMIMTFSI, it is hypothesized that the larger $TFSI^-$ anion might decompose over time, contrasting to the smaller and more mobile $EMIM^+$ cation, which could explain the observed distinct bending behavior.

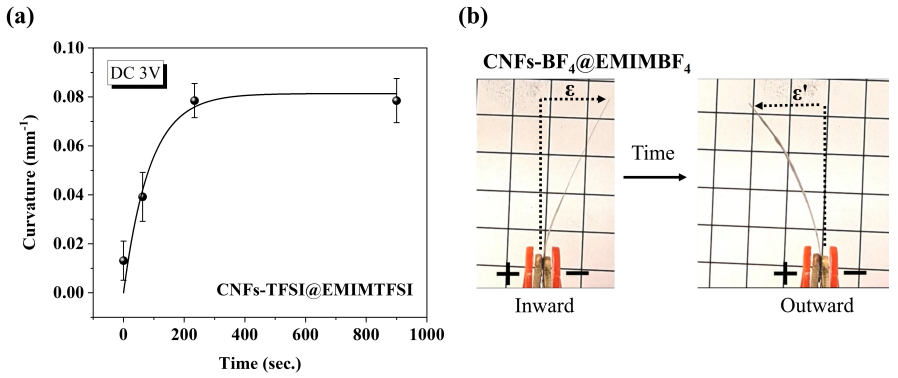

Figure 4.7. **(a)** CNFs-TFSI@EMIMTFSI actuator curvature kinetics under 3.0 V DC excitation. **(b)** Actuation behavior of CNFs-BF_4@EMIMBF_4 actuator under a 5.0 V DC excitation. Remodeled from Héraly et al. 2023.[66]

The CNFs-PF_6@EMIMPF_6 actuator exhibits a unique outward bending at both 3V and 5V, as shown in **Figure 4.8a**. This surprising behavior might be influenced by the solid-state nature of EMIMPF_6 at room temperature. Further investigation is required to fully understand these dynamics.

Under a 3.0 V AC square wave at 0.01 Hz, the CNFs-BF_4@EMIMBF_4 actuator outperforms the others. Its bending strain response is shown in **Figure 4.8b.** This good performance is due to the smaller BF_4^- anion, which facilitates rapid diffusion, advantageous in scenarios demanding quick adaptability in response to changes in polarizability.

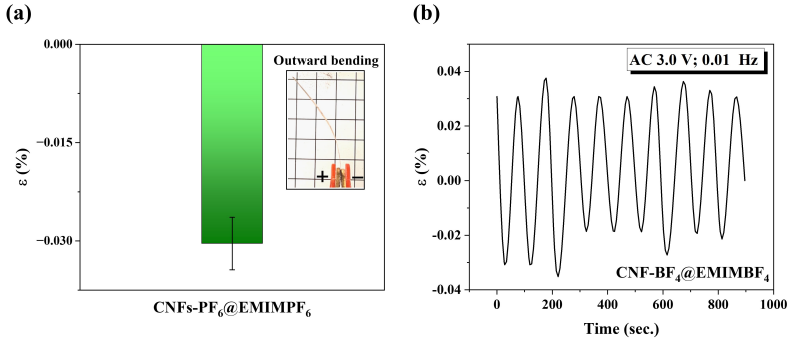

Figure 4.8. **(a)** Outward bending of the CNFs-PF_6@EMIMPF_6 actuator. **(b)** CNF-BF_4@EMIMBF_4 actuator response under a square wave function of 3.0 V and a frequency of 0.01 Hz. Remodeled from Héraly et al. 2023.[66]

4.6 Perspective

In this chapter, the focus is on exploring the role of voltage stimulus in controlling the actuation of CNFs actuators, which are crucial for applications requiring accurate motion such as artificial muscles and robotics. The study emphasizes the comparative impact of different electrolytes, specifically lithium-based salts and imidazolium-based ionic liquids, and their unique influences on actuator performance. Central to this analysis is the interaction between various anions (Cl^-, BF_4^-, $TFSI^-$, and PF_6^-) and the CNFs matrix, which significantly affects actuation behavior.

A notable observation is the superior performance of CNFs-TFSI@LiTFSI under both DC and AC conditions, highlighted by its significant bending strain and kinetic behavior. The study also reveals unique bending responses under varying voltage stimuli, driven by ion migration and its resulting volume expansion of the CNFs matrix in the electrode areas. This work underscores the importance of meticulous material and voltage selection in optimizing the function of CNFs-based actuators for future applications in soft robotics and bio-inspired devices.

5. Paper III: CO_2 Stimulus

In this section, the focus is on exploring the use of aminated cellulose nanofibrils in CO_2-responsive sensors.[74] It highlights the process of functionalizing CNFs to enhance their CO_2 capture capabilities, which is essential for the effectiveness of these sensors. The adaptability of CNFs and their potential in addressing environmental challenges are emphasized, aligning with the initial goal of investigating innovative and sustainable materials. This also highlights the practical implications of CNFs in the field of environmental science.[75]

5.1 Introduction

Functionalizing CNFs with primary amines enhances their ability to absorb CO_2 through a chemisorption process. When these aminated CNFs are processed into foam, they become suitable for use as dielectric layer in capacitive CO_2 sensor applications.[26,27] These advanced sensors have the ability to detect CO_2 in the environment and convert its presence into a measurable change, offering a promising approach for gas monitoring and environmental sensing.

5.2 Functionalizing CNFs with primary amines

Cellulose nanofibrils were treated with 3-aminopropyl(diethoxy)methylsilane (APDEMS) in water to graft primary amine groups onto their surface. The general scheme of this functionalization is depicted in **Figure 5.1**.

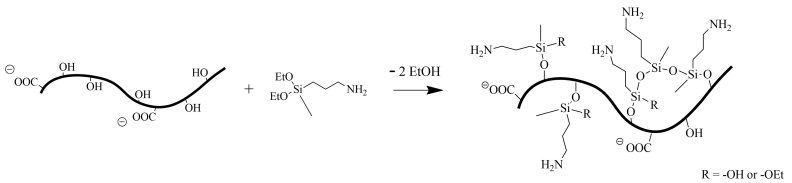

Figure 5.1. Schematic illustration of the APDEMS grafting process onto cellulose nanofibrils in an aqueous medium.

The grafted primary amines can react with CO_2 *via* chemisorption, forming ion pairs. Importantly, for sensor applications, this process is reversible when heat or vacuum is applied to desorb CO_2. Adding a strong base such as DBU to the system results in the formation of mobile protonated DBU, as it can easily capture proton during the reaction with CO_2.

The aminated CNFs were then freeze-dried into a foam, named FD-APDEMS-CNFs. The SEM image, as shown in **Figure 5.2a** provides insight into the foam's structure and reveals a network of interconnected pores with an observed average diameter of (31.1 ± 4.2) µm.

From the analysis of nitrogen (N_2) sorption isotherms, we elucidate the FD-APDEMS-CNFs foam with a low specific surface area (< 20 m^2/g) is macroporous. The large pores ensure the rapid diffusion of CO_2 gas inside the porous foam (**Figure 5.2b**).

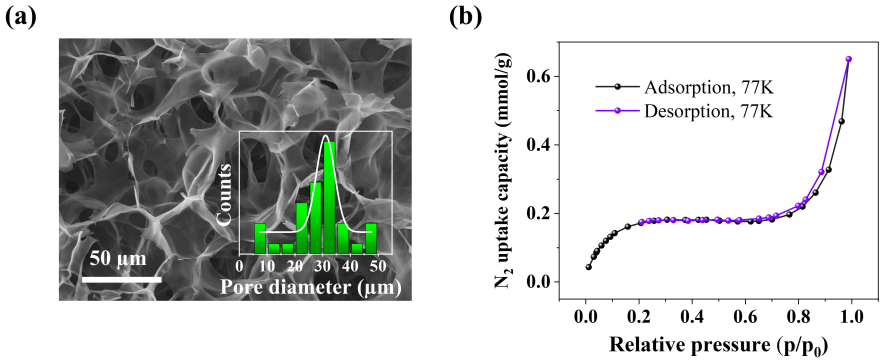

Figure 5.2. **(a)** Foam structure morphology visualized through SEM. **(b)** N_2 sorption isotherm of FD-APDEMS-CNFs.

5.3 CO_2-responsive sensor fabrication

The CO_2 sensor, designed as a parallel plate capacitor, incorporates three foam pieces. These foams are sandwiched between two aluminum foils and are secured with tape. This 3-foam configuration increases the device's contact area, consequently boosting its capacitance as outlined in **Equation 5.1**. To facilitate CO_2 desorption *via* infrared light (IR) heating, the aluminum foils are coated with a graphite ink to confer them with photothermal properties, as illustrated in **Figure 5.3**.

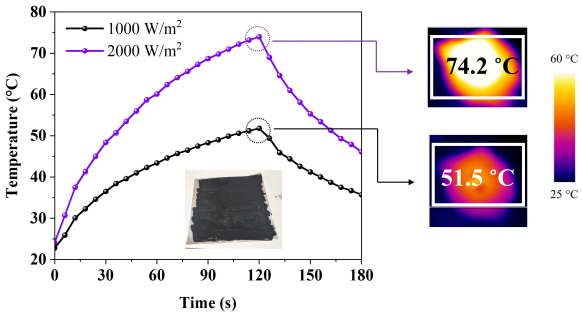

Figure 5.3. Evaluation of photothermal performance of the graphite ink-coated aluminum foil under IR irradiation of two different intensities (10^3 W/m² and 2×10^3 W/m²), assessed over two min, followed by a one-min temperature decrease recording.

The sensor's dielectric layer, pivotal for CO_2 sensitivity, is composed of FD-APDEMS-CNFs. The standard form, termed "aminated cellulose nanofibrils in the dielectric layer" (A-CNFs@DE), incorporates glycerol to improve the foam's plasticity and structural integrity. An alternative version, includes also DBU in the dielectric layer, which produces mobile cations during CO_2 adsorption,[76] and is named A-CNFs-DBU@DE. **Figure 5.4** showcases the assembly process, highlighting the incorporation of CNFs foams as dielectric layers situated between two graphite ink-coated aluminum foil electrodes.

Figure 5.4. Assembly of the CO_2-responsive sensor, displaying cellulose nanofibrils foams as dielectric layers between two aluminum foil electrodes

5.4 Analysis of operational mechanisms and performance

The capacitance of capacitor composed of A-CNFs@DE is closely linked to their dielectric constant. Exposure to CO_2 significantly boosts their polarization, primarily *via* the formation of negatively charged species, thereby enhancing the dielectric constant of the layer (**Figure 5.5a**). This increase directly leads to a rise in the capacitance of the sensor, as outlined in **Equation 5.1**.

$$C = \frac{\kappa \epsilon_0 A}{d}$$

Equation 5.1. This equation describes the capacitance of a plate capacitor, where C is the capacitance, κ the dielectric constant, ε_0 the vacuum permittivity, A the plate area, and d the plate separation.

The A-CNFs-DBU@DE sensor, incorporating DBU, further enhances these capacitive properties. The introduction of DBU leads to increased polarization upon CO_2 exposure due to the alignment of mobile protonated DBU cations in an electric field (**Figure 5.5b**). This results in an elevated dielectric constant, reduced voltage across the capacitor's plates, and consequently, increased capacitance.

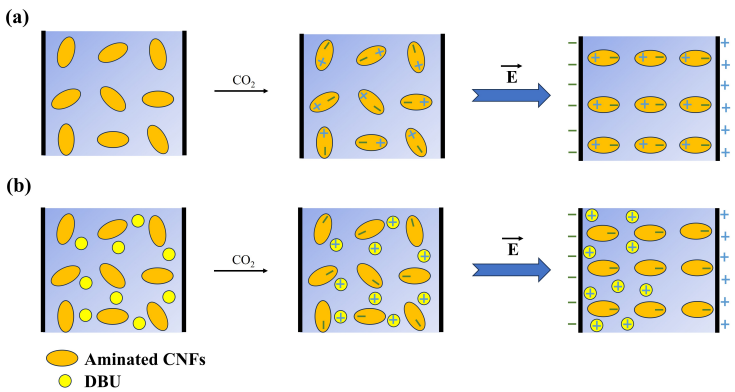

Figure 5.5. Illustration of the dielectric sensor's response to CO_2. **(a)** For A-CNFs@DE sensors, CO_2 exposure increases the CNFs' polarization, aligning the polarized A-CNFs toward the capacitor's charged plates, thereby enhancing capacitance. **(b)** The A-CNFs-DBU@DE sensor augments this response upon CO_2 exposure by effectively aligning mobile protonated DBU cations, thus increasing capacitance by reducing the effective voltage of the capacitor's charged plates.

Experimentally, this mechanism was confirmed. After a one-hour CO_2 desorption process at 90°C, the increase of capacitance over time for both sensors was evaluated under a two-hour CO_2 exposure at 400 ppm.

Namely, A-CNFs@DE's capacitance rose from 41 pF to 262 pF, while A-CNFs-DBU@DE exhibited a more dramatic increase from 500 pF to 5600 pF, as shown in **Figure 5.6**. This marked increase, attributed to the incorporation of DBU, significantly boosts the sensor's capacitance.

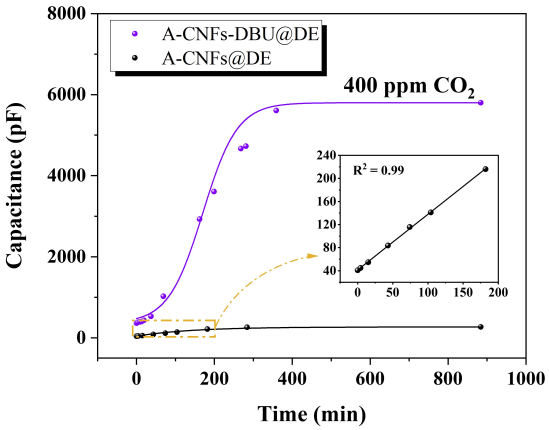

Figure 5.6. Capacitance-time profiles of A-CNFs@DE and A-CNFs-DBU@DE CO_2 sensors. The sensors' responses at 400 ppm CO_2, 35% RH, and a temperature of 21.0 °C are depicted, with an inset emphasizing the linear capacitance response observed within the first 200 minutes for the A-CNFs@DE sensor.

Additionally, the capacitance dynamic (ΔC) in a pure CO_2 atmosphere was investigated. This experiment highlighted the importance of good CO_2 capture in the dielectric layer for rapid capacitance changes, despite this capture being slow and the rate-determining factor even in a pure CO_2 environment. In this regard, the A-CNFs@DE sensor showed a stronger initial change in capacitance than the A-CNFs-DBU@DE sensor during the first 3 minutes (**Figure 5.7a**). This is attributed to its high CO_2 capture capacity of 2.2 mmol/g at 1 bar CO_2 (**Figure 5.7b**), leading to rapid CO_2 sorption and a swift capacitance increase. By contrast, A-CNFs-DBU@DE, with its lower 0.55 mmol/g CO_2 capture capacity, displayed a slower initial response.

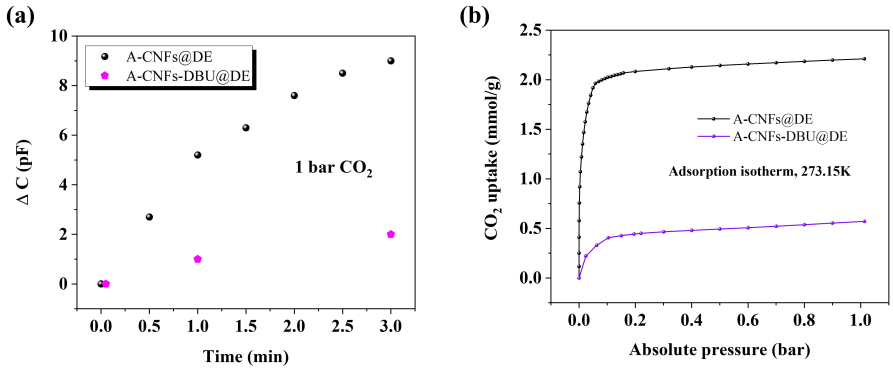

Figure 5.7. Comparative analysis of the two constructed sensors, showing **(a)** the change in capacitance within the first 3 minutes in a 1-bar CO_2 environment at 40% RH and 21.2 °C following the CO_2 desorption process, and **(b)** their CO_2 capture performance evaluated by gas sorption analysis measured at 273.15 K.

From experiments conducted in the ambient air and in pure CO_2 atmosphere, it is evident that a high capacity in CO_2 capture is beneficial for a quick change in capacitance over a short period. However, over time, the generation of mobile cations overtakes the CO_2 capture ability, resulting in a more intense capacitance change.

5.5 Perspective

These findings showcase the potential of functionalized CNFs for advanced gas monitoring and environmental sensing applications. The CO_2-responsive sensor is particularly well-suited for applications where it is imperative to maintain CO_2-free atmosphere. Its high sensitivity enables the detection of CO even at a low concentration of CO_2. For instance, the capacitance change can trigger a light indicator, providing a distinct visual alert of too high CO_2 levels. Furthermore, the photothermal properties of the sensor facilitate rapid CO_2 desorption, ensuring that the sensor can be quickly reset, making it ready for continuous and effective subsequent detection cycles.

6. General Discussion

In this thesis, a thorough investigation was conducted on stimuli-responsive materials derived from CNFs, covering applications that range from moisture-responsive actuators to advanced CO_2 sensors. Major achievements included:

- The development of moisture-responsive CNFs actuators, characterized by their swift bending and torsional movements in response to humidity changes.

- Thorough investigation into the effects of various electrolytes and anion types on the performance of CNFs-based actuators.

- The creation of a capacitive CO_2 sensor using amine-modified CNFs foam as an active component of the device.

The ease with which CNFs could be processed into diverse, robust structures such as films, foams, or fibers, coupled with their excellent functional versatility, including straightforward surface chemistry, allowing for the precise customization of their properties.

The operational principles of these stimuli-responsive materials varied depending on the specific stimulus. For moisture-responsive materials, the intrinsic hygroscopic nature of CNFs was leveraged. By contrast, voltage-responsive materials relied on ion migration within the CNFs matrix. Meanwhile, the key to the developed CO_2-responsive sensor was the chemical reaction between CO_2 and the primary amines in the CNFs.

Future work should focus on developing scalable and cost-effective manufacturing processes, and continue to advance research to enhance performance attributes such as speed, durability, and efficiency.

Acknowledgements

I am filled with profound gratitude as I reflect on my enriching journey as a doctoral candidate in the Department of Materials and Environmental Chemistry (MMK) at Stockholm University.

First and foremost, my profound thanks go to my supervisor, Jiayin, for his generosity, wisdom, unwavering patience, ceaseless positivity, and supportive guidance. His qualities and support have been the bedrock of my academic journey.

I also extend this feeling of gratitude to all my teammates for their collaboration in our research projects. Together, we have shared a passion for chemistry and the rich experiences that come with our cultural diversity.

Special thanks to Lennart for kindly taking on the role of co-supervisor, offering insightful discussions, and sharing his expertise.

I would like to express my sincere acknowledgments to all the talented researchers (Mirva, Cheuk-Wai, Ken, Kjell, Zoltan, and many others) who trained me on various instruments, and to the administration team and all colleagues and friends. Their contributions have been instrumental to my academic growth, making this journey both fruitful and thoroughly enjoyable.

Lastly, thank you to my family, my source of love, strength, and inspiration. Their support, constant encouragement, and faith in my abilities have served as my guiding light.

References

1 Wei, M., Gao, Y., Li, X. & Serpe, M. Stimuli-responsive polymers and their applications. *Polymer Chemistry* **8**, 127-143 (2017).

2 Mrinalini, M. & Prasanthkumar, S. Recent advances on stimuli‐responsive smart materials and their applications. *ChemPlusChem* **84**, 1103-1121 (2019).

3 Ali, S. H. The materials science imperative in meeting the Sustainable Development Goals. *Nature Materials* **17**, 1052-1053 (2018).

4 Klemm, D. *et al.* Nanocelluloses: a new family of nature‐based materials. *Angewandte Chemie* **50**, 5438-5466 (2011).

5 Nevell, T. P. & Zeronian, S. H. Cellulose chemistry and its applications. (1985).

6 Zhang, J. & Zhang, J. Advanced functional materials based on cellulose. *Acta Polym Sin* **12**, 1376-1398 (2010).

7 Ramamoorthy, S. K., Skrifvars, M. & Persson, A. A review of natural fibers used in biocomposites: Plant, animal and regenerated cellulose fibers. *Polymer Reviews* **55**, 107-162 (2015).

8 Klemm, D., Heublein, B., Fink, H. P. & Bohn, A. Cellulose: fascinating biopolymer and sustainable raw material. *Angewandte Chemie* **44**, 3358-3393 (2005).

9 Huang, Y.-B. & Fu, Y. Hydrolysis of cellulose to glucose by solid acid catalysts. *Green Chemistry* **15**, 1095-1111 (2013).

10 Van De Ven, T. G. & Godbout, L. *Cellulose: fundamental aspects*. (BoD–Books on Demand, 2013).

11 Li, T. *et al.* Developing fibrillated cellulose as a sustainable technological material. *Nature* **590**, 47-56 (2021).

12 Nechyporchuk, O., Belgacem, M. N. & Bras, J. Production of cellulose nanofibrils: A review of recent advances. *Industrial Crops and Products* **93**, 2-25 (2016).

13 Isogai, A., Saito, T. & Fukuzumi, H. TEMPO-oxidized cellulose nanofibers. *Nanoscale* **3**, 71-85 (2011).

14 Theato, P., Sumerlin, B. S., O'Reilly, R. K. & Epps III, T. H. Stimuli responsive materials. *Chemical Society Reviews* **42**, 7055-7056 (2013).

15 Deen, G. R. & Loh, X. J. Stimuli-responsive cationic hydrogels in drug delivery applications. *Gels* **4**, 13 (2018).

16 Ali, I. *et al.* A review of electro-stimulated gels and their applications: Present state and future perspectives. *Materials Science and Engineering: C* **103**, 109852 (2019).

17 Zhang, Q. *et al.* An all-organic composite actuator material with a high dielectric constant. *Nature* **419**, 284-287 (2002).
18 Kim, J. *et al.* Review of soft actuator materials. *International Journal of Precision Engineering Manufacturing* **20**, 2221-2241 (2019).
19 Apsite, I., Salehi, S. & Ionov, L. Materials for smart soft actuator systems. *Chemical Reviews* **122**, 1349-1415 (2021).
20 Li, M., Pal, A., Aghakhani, A., Pena-Francesch, A. & Sitti, M. Soft actuators for real-world applications. *Nature Reviews Materials* **7**, 235-249 (2022).
21 Noguchi, T. & Tsumori, F. Soft actuator with large volumetric change using vapor–liquid phase transition. *Japanese Journal of Applied Physics* **59**, SIIL08 (2020).
22 Kularatne, R. S., Kim, H., Boothby, J. M. & Ware, T. H. Liquid crystal elastomer actuators: Synthesis, alignment, and applications. *Journal of Polymer Science Part B: Polymer Physics* **55**, 395-411 (2017).
23 Hu, Y. *et al.* Self-locomotive soft actuator based on asymmetric microstructural $Ti_3C_2T_X$ MXene film driven by natural sunlight fluctuation. *ACS Nano* **15**, 5294-5306 (2021).
24 Hu, L., Zhang, Q., Li, X. & Serpe, M. J. J. M. H. Stimuli-responsive polymers for sensing and actuation. *Materials Horizons* **6**, 1774-1793 (2019).
25 Janata, J. Chemical sensors. *Analytical Chemistry* **64**, 196-219 (1992).
26 Boudaden, J., Klumpp, A., Endres, H.-E. & Eisele, I. in *Proceedings.* 472 (MDPI).
27 Boudaden, J., Klumpp, A., Eisele, I. & Kutter, C. in *2016 IEEE Sensors.* 1-3 (IEEE).
28 Liao, B., Wei, Q., Wang, K. & Liu, Y. Study on CuO–$BaTiO_3$ semiconductor CO_2 sensor. *Sensors and Actuators B: Chemical* **80**, 208-214 (2001).
29 Khatib, M. & Haick, H. Sensors for volatile organic compounds. *ACS Nano* **16**, 7080-7115 (2022).
30 Wencel, D., Abel, T. & McDonagh, C. Optical chemical pH sensors. *Analytical Chemistry* **86**, 15-29 (2014).
31 Li, Z., Yang, X., Li, W. & Liu, H. Stimuli-responsive cellulose paper materials. *Carbohydrate Polymers* **210**, 350-363 (2019).
32 Chen, W., Sun, B., Biehl, P. & Zhang, K. Cellulose‐based soft actuators. *Macromolecular Materials and Engineering* **307**, 2200072 (2022).
33 Wang, J., Wang, L., Gardner, D. J., Shaler, S. M. & Cai, Z. Towards a cellulose-based society: opportunities and challenges. *Cellulose* **28**, 4511-4543 (2021).
34 Kim, J., Yun, S. & Ounaies, Z. Discovery of Cellulose as a Smart Material. *Macromolecules* **39**, 5583-5583 (2006).

35 Zhu, Q. *et al.* Bioinspired smart moisture actuators based on nanoscale cellulose materials and porous, hydrophilic EVOH nanofibrous membranes. *ACS Applied Materials & Interfaces* **11**, 1440-1448 (2018).
36 Chemin, M., Beaumal, B., Cathala, B. & Villares, A. Ph-responsive properties of asymmetric nanopapers of nanofibrillated cellulose. *Nanomaterials* **10**, 1380 (2020).
37 Hassan, S. *et al.* Review of cellulose smart material: biomass conversion process and progress on cellulose-based electroactive paper. *Journal of Renewable Materials* **6**, 1-25 (2018).
38 Teeri, T. T., Brumer, H., Daniel, G. & Gatenholm, P. Biomimetic engineering of cellulose-based materials. *Trends in Biotechnology* **25**, 299-306 (2007).
39 Zhao, D. *et al.* Cellulose‐based flexible functional materials for emerging intelligent electronics. *Advanced Materials* **33**, 2000619 (2021).
40 Petersen, N. & Gatenholm, P. Bacterial cellulose-based materials and medical devices: current state and perspectives. *Applied Microbiology and Biotechnology* **91**, 1277-1286 (2011).
41 Ummartyotin, S. & Manuspiya, H. A critical review on cellulose: From fundamental to an approach on sensor technology. *Renewable and Sustainable Energy Reviews* **41**, 402-412 (2015).
42 Teodoro, K. B. *et al.* A review on the role and performance of cellulose nanomaterials in sensors. *ACS Sensors* **6**, 2473-2496 (2021).
43 Saito, T., Kimura, S., Nishiyama, Y. & Isogai, A. Cellulose nanofibers prepared by TEMPO-mediated oxidation of native cellulose. *Biomacromolecules* **8**, 2485-2491 (2007).
44 Pei, A., Butchosa, N., Berglund, L. A. & Zhou, Q. Surface quaternized cellulose nanofibrils with high water absorbency and adsorption capacity for anionic dyes. *Soft Matter* **9**, 2047-2055 (2013).
45 William, S., Hummers, J. & Offeman, R. E. Preparation of graphitic oxide. *Journal of the American Chemical Society* **80**, 1339 (1958).
46 Héraly, F. *et al.* Nanodancing with Moisture: Humidity‐Sensitive Bilayer Actuator Derived from Cellulose Nanofibrils and Reduced Graphene Oxide. *Advanced Intelligent Systems*, 2100084 (2021).
47 Barrett, E. P., Joyner, L. G. & Halenda, P. P. The determination of pore volume and area distributions in porous substances. I. Computations from nitrogen isotherms. *Journal of the American Chemical Society* **73**, 373-380 (1951).
48 Landers, J., Gor, G. Y. & Neimark, A. V. Density functional theory methods for characterization of porous materials. *Colloids and Surfaces A: Physicochemical and Engineering Aspects* **437**, 3-32 (2013).

49 Pu, W., Wei, F., Yao, L. & Xie, S. A review of humidity-driven actuator: toward high response speed and practical applications. *Journal of Materials Science* **57**, 12202-12235 (2022).
50 Huang, P., Wang, C., Huang, Y. & Wu, M. Structure and properties of cellulose nanofibrils. *Nanocellulose: From Fundamentals to Advanced Materials*, 53-80 (2019).
51 Saito, T. *et al.* Individualization of nano-sized plant cellulose fibrils by direct surface carboxylation using TEMPO catalyst under neutral conditions. *Biomacromolecules* **10**, 1992-1996 (2009).
52 Lv, P., Lu, X., Wang, L. & Feng, W. Nanocellulose‐Based Functional Materials: From Chiral Photonics to Soft Actuator and Energy Storage. *Advanced Functional Materials*, 2104991 (2021).
53 Aziz, S. & Spinks, G. M. Torsional artificial muscles. *Materials Horizons* **7**, 667-693 (2020).
54 Lundahl, M. J. *Wet spinning of CNF hydrogels* Aalto University, (2018).
55 Haines, C. S. *et al.* New twist on artificial muscles. *Proceedings of the National Academy of Sciences* **113**, 11709-11716 (2016).
56 Dai, M. *et al.* Humidity-responsive bilayer actuators based on a liquid-crystalline polymer network. *ACS Applied Materials & Interfaces* **5**, 4945-4950 (2013).
57 Gong, J., Lin, H., Dunlop, J. W. & Yuan, J. Hierarchically arranged helical fiber actuators derived from commercial cloth. *Advanced Materials* **29**, 1605103 (2017).
58 Haines, C. S. *et al.* Artificial muscles from fishing line and sewing thread. *Science* **343**, 868-872 (2014).
59 Shahinpoor, M. & Kim, K. J. Solid-state soft actuator exhibiting large electromechanical effect. *Applied Physics Letters* **80**, 3445-3447 (2002).
60 Bar-Cohen, Y. & Anderson, I. A. J. M. o. S. M. Electroactive polymer (EAP) actuators—background review. *Mechanics of Soft Materials* **1**, 1-14 (2019).
61 Bar-Cohen, Y. *Electroactive polymer (EAP) actuators as artificial muscles: reality, potential, and challenges*. Vol. 136 (SPIE press, 2004).
62 Bar-Cohen, Y. in *Electroactive Polymer Actuators and Devices (EAPAD) XXII.* 1137502 (International Society for Optics and Photonics).
63 Khuyen, N. Q. *et al.* Comparative analysis of fluorinated anions for polypyrrole linear actuator electrolytes. *Polymers* **11**, 849 (2019).
64 Zhu, G. & Lin, N. Surface chemistry of nanocellulose. *Nanocellulose: from fundamentals to advanced materials*, 115-153 (2019).
65 Fukuzumi, H., Saito, T. & Isogai, A. Influence of TEMPO-oxidized cellulose nanofibril length on film properties. *Carbohydrate Polymers* **93**, 172-177 (2013).

66 Héraly, F., Pang, B. & Yuan, J. Cationic Cellulose Nanofibrils-based electro-actuators: the effects of counteranion and electrolyte. *Sensors and Actuators Reports*, 100142 (2023).
67 Zhang, S. S. A review on electrolyte additives for lithium-ion batteries. *Journal of Power Sources* **162**, 1379-1394 (2006).
68 Kim, J.-K., Matic, A., Ahn, J.-H. & Jacobsson, P. An imidazolium based ionic liquid electrolyte for lithium batteries. *Journal of Power Sources* **195**, 7639-7643 (2010).
69 Holbrey, J. D. & Seddon, K. Ionic liquids. *Clean Products and Processes* **1**, 223-236 (1999).
70 Forsyth, S. A., Pringle, J. M. & MacFarlane, D. R. Ionic liquids—an overview. *Australian Journal of Chemistry* **57**, 113-119 (2004).
71 Galiński, M., Lewandowski, A. & Stępniak, I. Ionic liquids as electrolytes. *Electrochimica Acta* **51**, 5567-5580 (2006).
72 McEwen, A. B., Ngo, H. L., LeCompte, K. & Goldman, J. L. Electrochemical properties of imidazolium salt electrolytes for electrochemical capacitor applications. *Journal of the Electrochemical Society* **146**, 1687 (1999).
73 Zhao, Y. H., Abraham, M. H. & Zissimos, A. M. Determination of McGowan volumes for ions and correlation with van der Waals volumes. *Journal of Chemical Information Computer Sciences* **43**, 1848-1854 (2003).
74 Wu, J. *et al.* In situ μ-printed optical fiber-tip CO_2 sensor using a photocrosslinkable poly (ionic liquid). *Sensors and Actuators B: Chemical* **259**, 833-839 (2018).
75 Shatkin, J. A. & Kim, B. Cellulose nanomaterials: life cycle risk assessment, and environmental health and safety roadmap. *Environmental Science: Nano* **2**, 477-499 (2015).
76 Hedayati, A. & Feyzi, F. Towards water-insensitive CO_2-binding organic liquids for CO_2 absorption: Effect of amines as promoter. *Journal of Molecular Liquids* **306**, 112938 (2020).